ESI Updated - 12th May 2020

Silica-supported, narrowly distributed, subnanometric Pt–Zn particles from single sites with high propane dehydrogenation performance

Lukas Rochlitz,[†] Keith Searles,[†] Jan Alfke,[§,†] Dmitry Zemlyanov,[‡] Olga V. Safonova,[§]

Christophe Copéret,[*,†]

[†]Department of Chemistry and Applied Biosciences, ETH Zürich, Vladimir-Prelog-Weg 1-5, CH-8093 Zürich, Switzerland

[‡] Birck Nanotechnology Center, Purdue University, 1205 West State Street, West Lafayette, Indiana 47907, United States

§ Paul Scherrer Institut, CH-5232 Villigen, Switzerland

Experimental

All operations were performed in a M. Braun glove box under an argon atmosphere or using high vacuum and standard Schlenk techniques. Pentane was purged with argon for 30 minutes and dried using a MB SPS 800 solvent purification system where columns used for pentane purification were packed with activated alumina. Benzene and deuterated benzene (C6D6) were vacuum distilled from purple Na^0/benzophenone. All solvents were stored over 4 Å molecular sieves after being transferred to a glove box. Celite and 4 Å molecular sieves were activated under high vacuum overnight at 350 °C. $SiO_{2\text{-}700}$ was prepared by heating Degauss Aerosil (200 m^2/g) to 500 °C (300 °C/h), calcining in air for 12 hours, evacuating to high vacuum (10^{-5} mbar) keeping 500 °C for 8 hours, heating to 700 °C (60 °C/h), and maintaining 700 °C for 24 hours. Titration of the $SiO_{2\text{-}700}$ using $[Mg(CH_2Ph)_2(THF)_2]$ purified *via* sublimation prior to use, yielded an Si-OH density of 0.3 mmol/g, corresponding to 0.9 accessible Si-OH groups per nm^2. The molecular complexes $[Zn(OSi(OtBu)_3)_2]_2$ and $[Pt(OSi(OtBu)_3)_2(COD)]$ were prepared according to literature procedures.[1,2] All other reagents were purchased from Sigma-Aldrich or Acros Organics and used as received. The supported species **Zn^{II}/SiO_2** and supported platinum nanoparticles **Pt^0/SiO_2** (Elemental Analysis: Pt, 3.96%) were prepared according to literature procedures.[3,4] Transmission IR spectra were recorded using a Bruker Alpha FT-IR spectrometer. Solid-state NMR spectra were recorded on a Bruker 400 MHz NMR spectrometer using a triple resonance 4 mm CP-MAS probe. Samples were packed in 4 mm zirconia rotors and referenced to adamantine at 38.44 ppm. Mikroanalytisches Labor Pascher located in Remagen, Germany performed elemental analyses.

Synthesis of $Zn(OSi(OtBu)_3)/SiO_2$

$SiO_{2\text{-}700}$ (1.733 g, 0.537 mmol -OH) was added to a 100 ml Schlenk flask. Benzene (about 10 ml) was added slowly while stirring to give a white suspension. **$Zn(OSi(OtBu)_3)_2$** (0.316 g, 0.534 mmol) was added slowly to the suspension as a white solution in benzene (about 5 ml) while stirring (100 rpm). The resulting suspension was stirred for 12 h at rt. The benzene on top of the silica material was decanted and the material washed with benzene (10 ml) three times to wash off unreacted complex. The material was then washed with pentane before it was dried under high vacuum (10^{-5} mbar) for 4 h to remove residual solvent yielding a white solid. ^{1}H NMR spectroscopy (300 MHz, 25 °C, d1 = 60 sec) of the combined washing solutions (only the benzene solutions) using ferrocene as internal standard identified $HOSi(OtBu)_3$ (0.307 mmol, 0.57 Zn_{added}^{-1}) as well as isobutene (0.226 mmol, 0.075 mmol $HOSi(OtBu)_3$ equiv, 0.14 Zn_{added}^{-1}), suggesting a grafted Zn amount of 0.71 equiv. Elemental Analysis: Zn, 1.67; C, 4.46; H, 0.91.

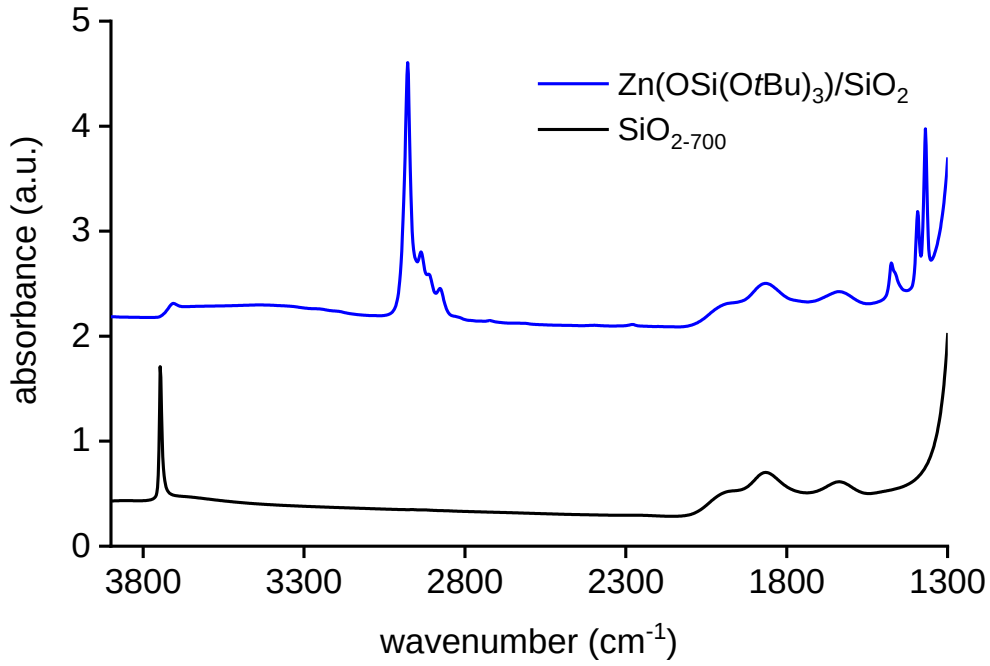

Figure S1. Transmission IR spectra of **$SiO_{2\text{-}700}$** (bottom) and **$Zn(OSi(OtBu)_3)/SiO_2$** (top) normalized to the $\upsilon_{Si\text{-}O}$ vibrational frequency at 1865 cm^{-1}.

Synthesis of Zn^{II}/SiO_2

$Zn(OSi(OtBu)_3)/SiO_2$ (1.733 g) was added to a tubular quartz reactor. The reactor was set under high vacuum (10^{-5} mbar) and successively heated to 300 °C (5 °C/min) for 1 h, 400 °C (5 °C/min) for 1 h, 500 °C (5 °C/min) for 1 h, 600 °C (5 °C/min) for 8 h yielding a white solid. ^{1}H NMR spectroscopy (300 MHz, 25 °C, d1 = 60 sec) of the volatiles released during the thermolytic treatment using ferrocene as internal standard identified isobutene (1.517 mmol, 0.506 mmol $HOSi(OtBu)_3$ equiv, 0.94 Zn_{added}^{-1}), *tert*-butanol (0.178 mmol, 0.059 $HOSi(OtBu)_3$ equiv, 0.11 Zn_{added}^{-1}) as well as $HOSi(OtBu)_3$ (0.012 mmol, 0.02 Zn_{added}^{-1}). This suggests a grafted Zn amount of 1.07 equiv. Elemental Analysis: Zn, 1.73.

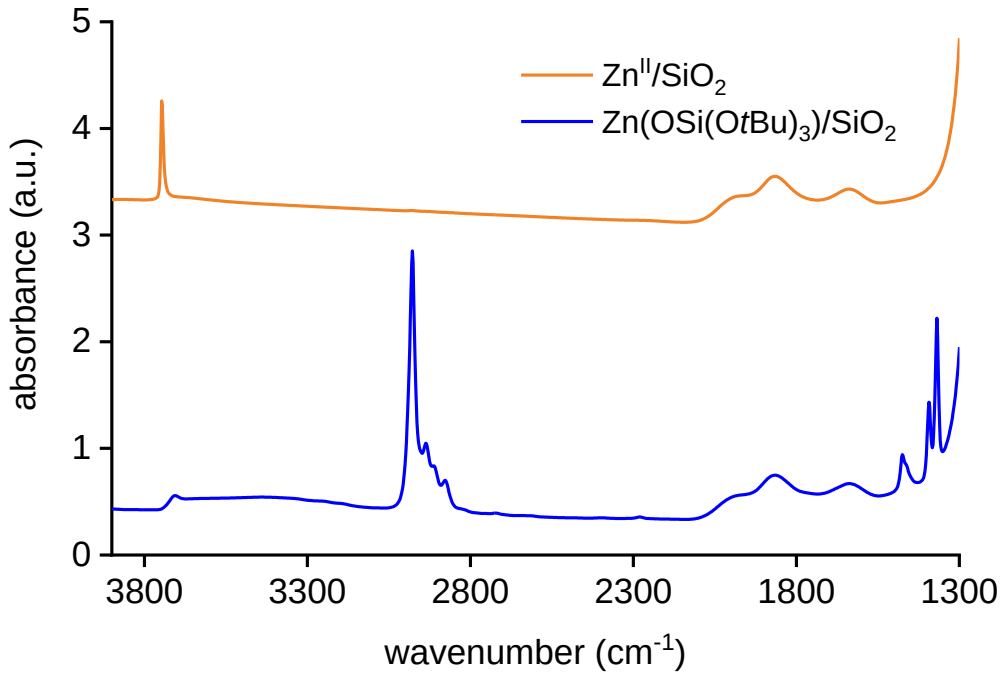

Figure S2. Transmission IR spectra of **$Zn(OSi(OtBu)_3)/SiO_2$** (bottom) and **Zn^{II}/SiO_2** (top) normalized to the $\upsilon_{Si\text{-}O}$ vibrational frequency at 1865 cm^{-1}.

Synthesis of $Pt(OSi(OtBu)_3(COD)Zn^{II}/SiO_2$

Zn^{II}/SiO2 (0.306 g, 0.067 mmol -OH) was added to a 100 ml Schlenk flask. Benzene (about 5 ml) was added slowly while stirring to give a white suspension. **$Pt(OSi(OtBu)_3)_2(COD)$** (0.066 g, 0.080 mmol) was added dropwise to the suspension as a colorless solution in benzene (about 10 ml) while stirring (100 rpm). The resulting white suspension was stirred for 12 h at rt. The benzene on top of the silica material was decanted and the material washed with benzene (10 ml) three times to wash off unreacted complex. The material was then washed with pentane before it dried under high vacuum (10^{-5} mbar) for 5 h to remove residual solvent yielding a white solid. ^{1}H NMR spectroscopy (300 MHz, 25 °C, d1 = 60 sec) of the combined washing solutions (only the three benzene solutions) using ferrocene as internal standard identified remaining $Pt(OSi(OtBu)_3)_2(COD)$ (0.028 mmol, 0.35 Pt_{added}^{-1}) as well as $HOSi(OtBu)_3$ (0.028 mmol, 0.35 Pt_{added}^{-1}). Elemental Analysis: Zn, 1.62; Pt, 2.90; C, 4.44; H, 0.79.

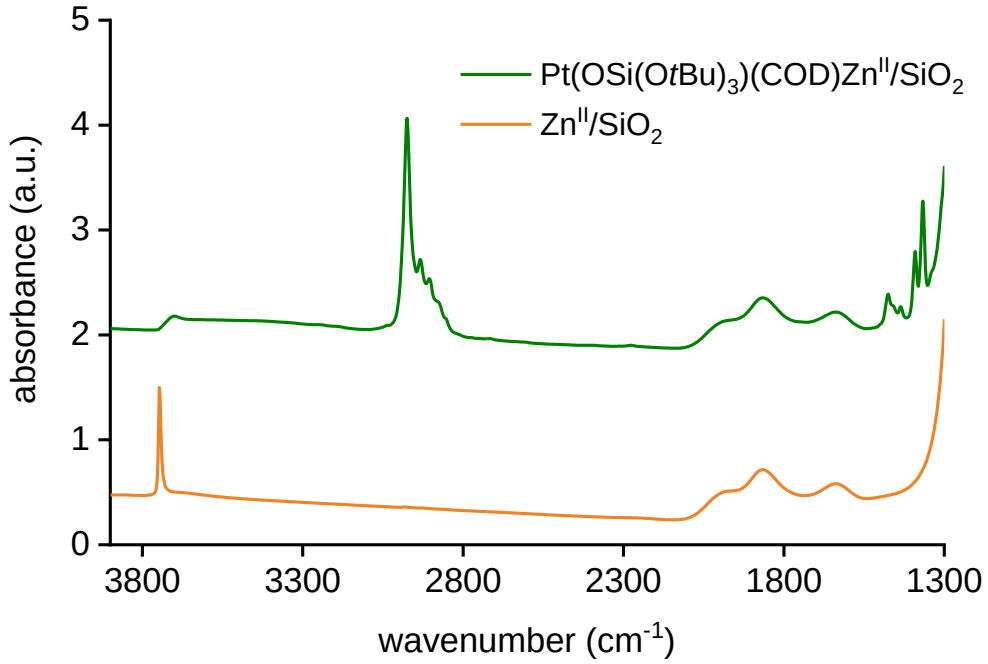

Figure S3. Transmission IR spectra of **Zn^{II}/SiO_2** (bottom) and **$Pt(OSi(OtBu)_3)_2(COD)Zn^{II}/SiO_2$** (top) normalized to the $\upsilon_{Si\text{-}O}$ vibrational frequency at 1865 cm^{-1}.

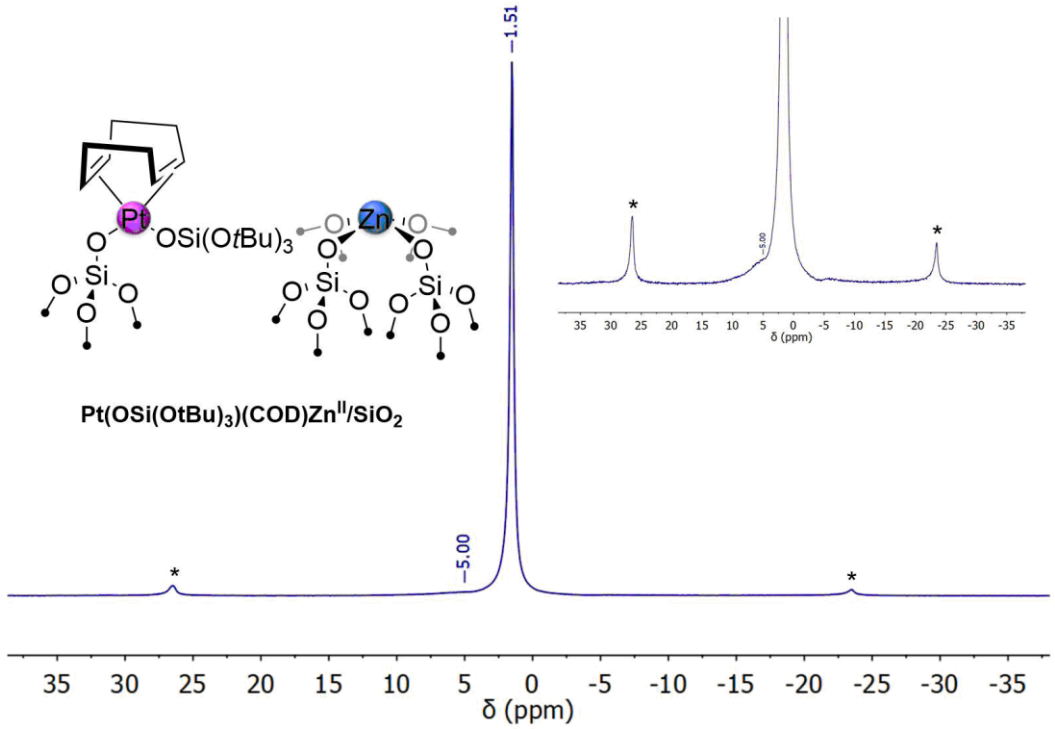

Figure S4. ^{1}H SSNMR spectrum of **Pt(OSi(OtBu)$_3$)$_2$(COD)Zn^{II}/SiO$_2$** (spinning rate, 10 kHz; scans, 16). Spinning side bands are indicated with a *.

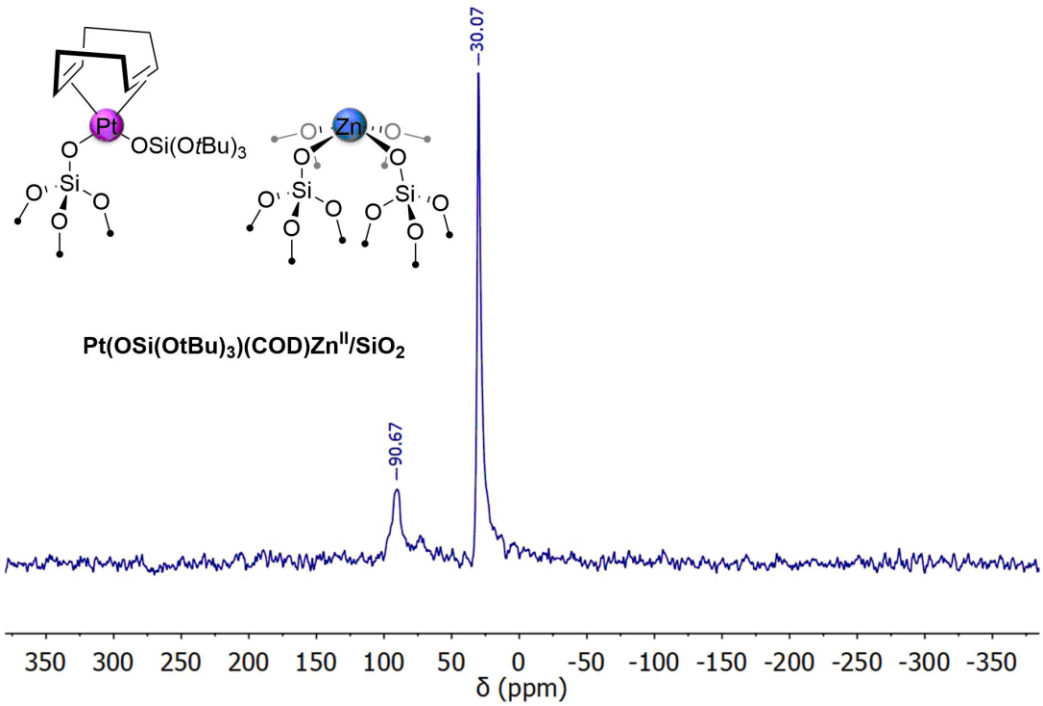

Figure S5. ^{13}C SSNMR spectrum of **Pt(OSi(OtBu)$_3$)$_2$(COD)Zn^{II}/SiO$_2$** (spinning rate, 10 kHz; scans, 14472; contact time, 2 ms).

Synthesis of $Pt^0Zn^{\delta+}/SiO_2$

$Pt(OSi(OtBu)_3)_2(COD)Zn^{II}/SiO_2$ (1.055 g) was added to a tubular quartz flow-reactor supported with a porous quartz frit. The reactor was heated to 600 °C (5 °C/min) for 8 h under a steady flow of H_2. The reactor was subsequently evacuated under high vacuum (10^{-5} mbar) while cooling to rt to yield a dark material. Elemental Analysis: Zn, 1.54; Pt, 3.05; C, 0.17; H, 0.11.

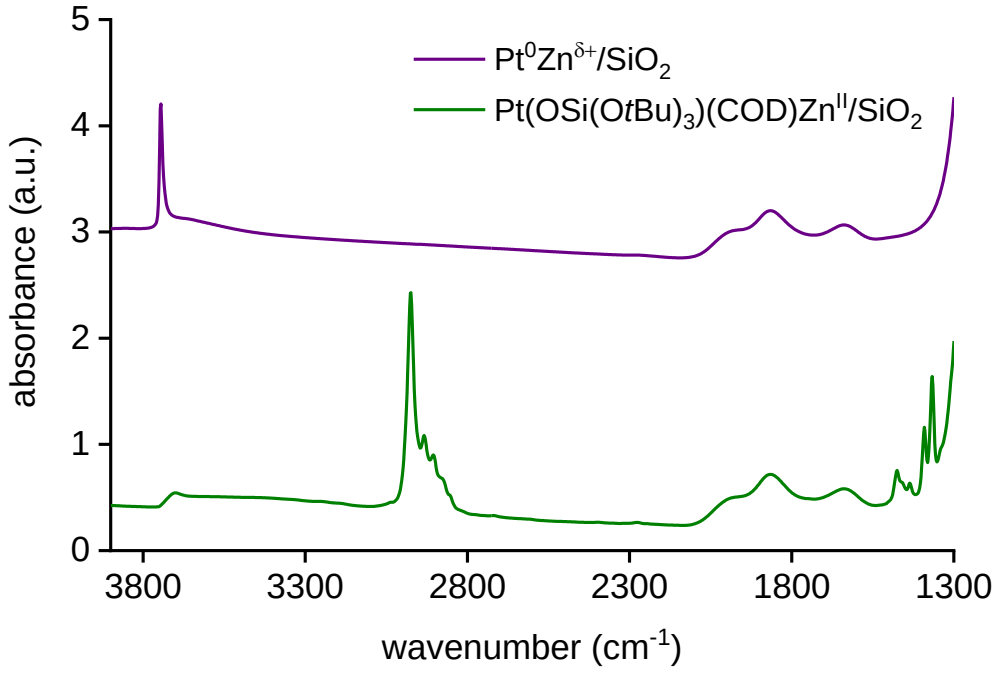

Figure S6. Transmission IR spectra of **$Pt(OSi(OtBu)_3)_2(COD)Zn^{II}/SiO_2$** (bottom) and **$Pt^0Zn^{\delta+}/SiO_2$** (top) normalized to the $\upsilon_{Si\text{-}O}$ vibrational frequency at 1865 cm^{-1}.

TEM Studies.

TEM and STEM images were recorded on a FEI Talos F200X instrument. Powdered samples were mixed in solid form with a Lacey-C 300 mesh Cu grid inside of a glovebox under an atmosphere of Ar before mounted on a vacuum transfer tomography holder from Fischione Instruments (model #2560) inside the glove box which was subsequently transferred to the chamber of the Microscope in the absence of air.

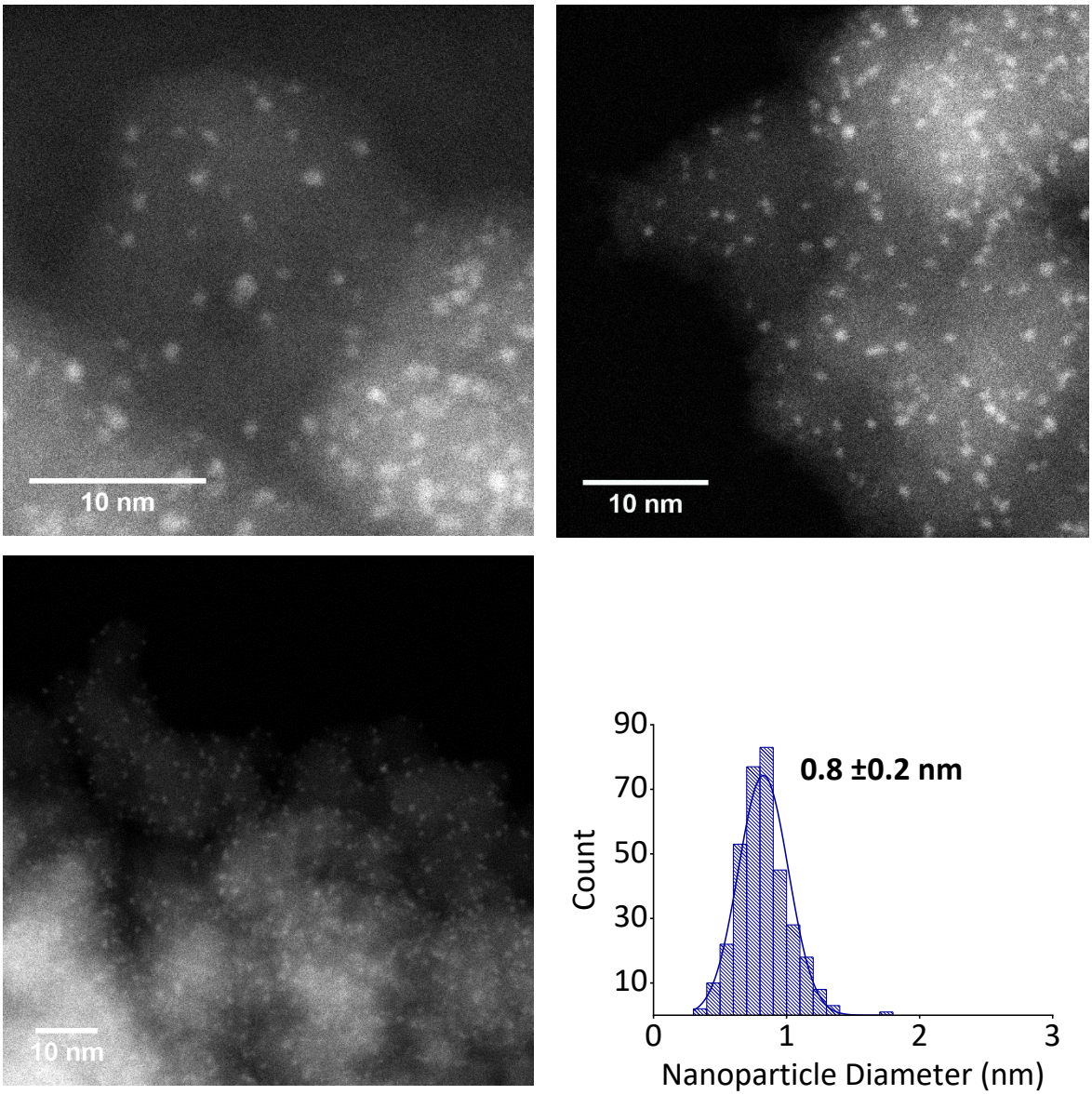

Figure S7. HAADF-STEM images of $\mathbf{Pt^0Zn^{\delta+}/SiO_2}$ and particle size distribution.

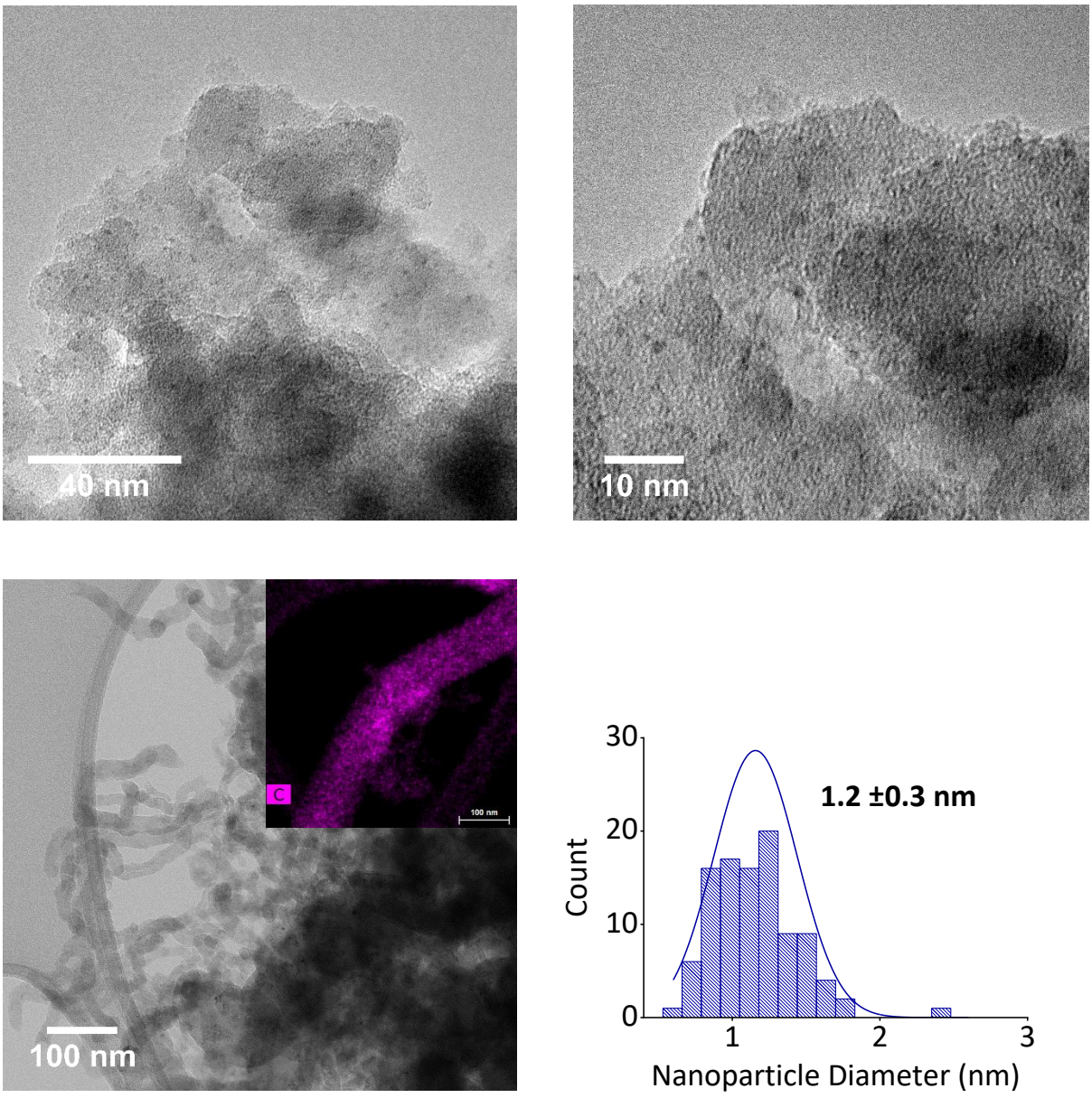

Figure S8. TEM images of spent $Pt^0Zn^{\delta+}/SiO_2$ (30 h on stream) including EDX analysis of the sample and particle size distribution.

FTIR Adsorption Studies.

CO adsorption IR studies.

Self-supporting pellets of **Zn^{II}/SiO_2**, **Pt^0/SiO_2** and **$Pt^0Zn^{\delta+}/SiO_2$** were freshly prepared, submitted to an atmosphere of CO and analyzed by transmission infrared spectroscopy at 2 cm^{-1} resolution. For the Pt containing pellets the mass (ca. 2-3 mg) and CO pressures (ca. 10-11 mbar) were kept low to prevent saturation of the spectra. For the Zn containing samples pellets with higher mass (10-11 mg) and pressures (120 mbar) were prepared. After placing each sample under high vacuum (10^{-5} mbar), the pellet was exposed to CO and subsequently analyzed by infrared spectroscopy. High vacuum (10^{-5} mbar) was also applied at room temperature after CO exposure to study the reversibility of CO binding. All pressures were maintained for a minimum of 5 minutes prior to analysis by infrared spectroscopy.

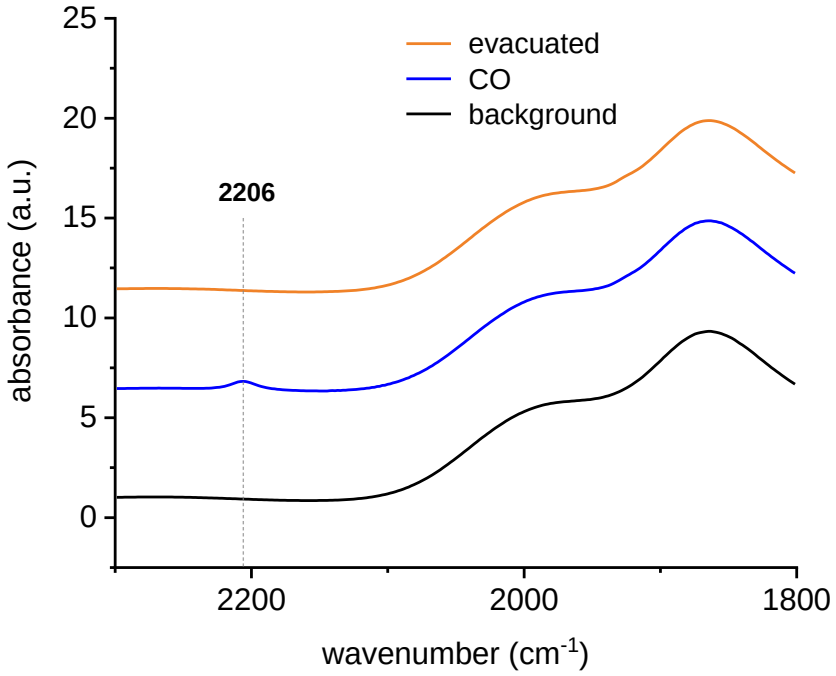

Figure S9. CO adsorption on **Zn^{II}/SiO_2**. The spectra are offset and normalized to the $\upsilon_{Si\text{-}O}$ vibrational frequency at 1865 cm^{-1}.

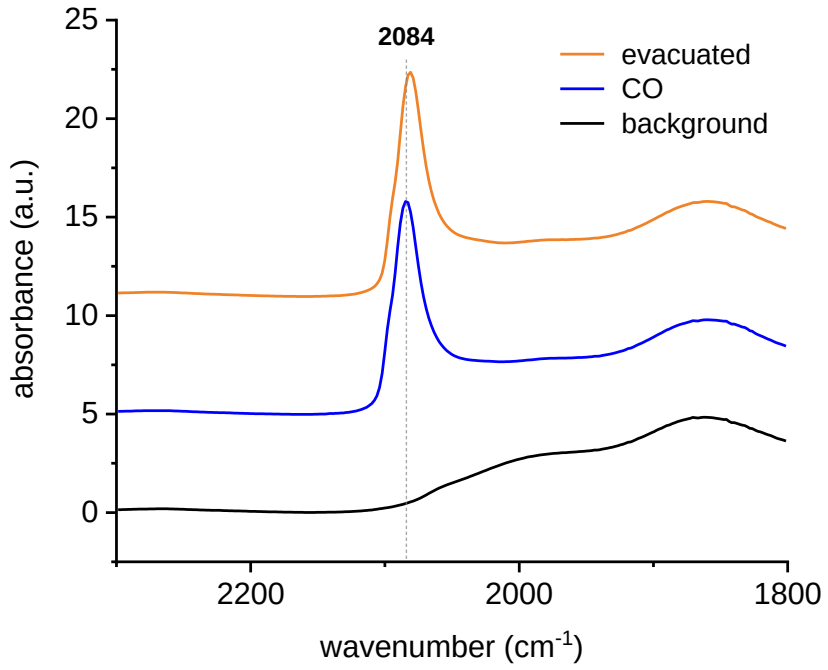

Figure S10. CO adsorption on **Pt^0/SiO_2**. The spectra are offset and normalized to the $\upsilon_{Si\text{-}O}$ vibrational frequency at 1865 cm^{-1}.

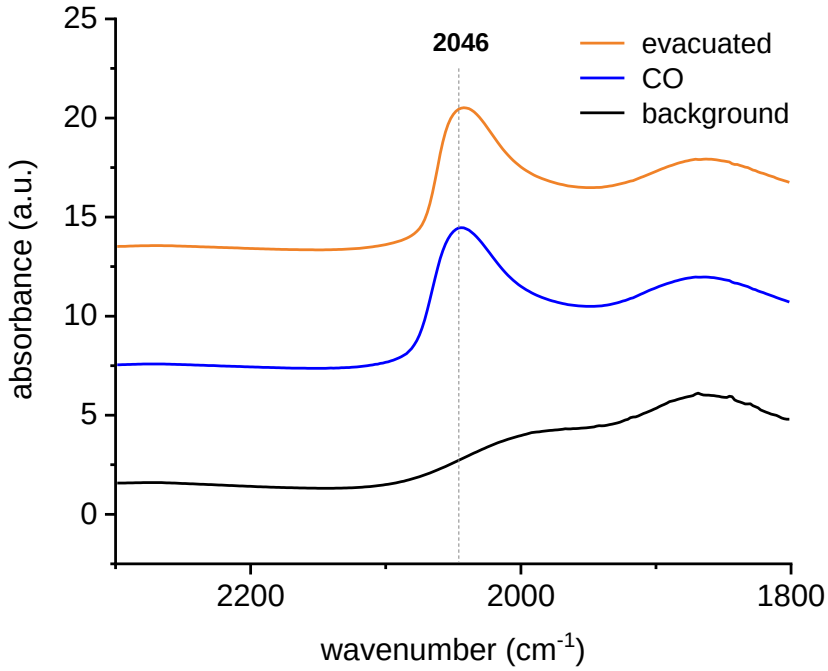

Figure S11. CO adsorption on **$Pt^0Zn^{\delta+}/SiO_2$**. The spectra are offset and normalized to the $\upsilon_{Si\text{-}O}$ vibrational frequency at 1865 cm^{-1}.

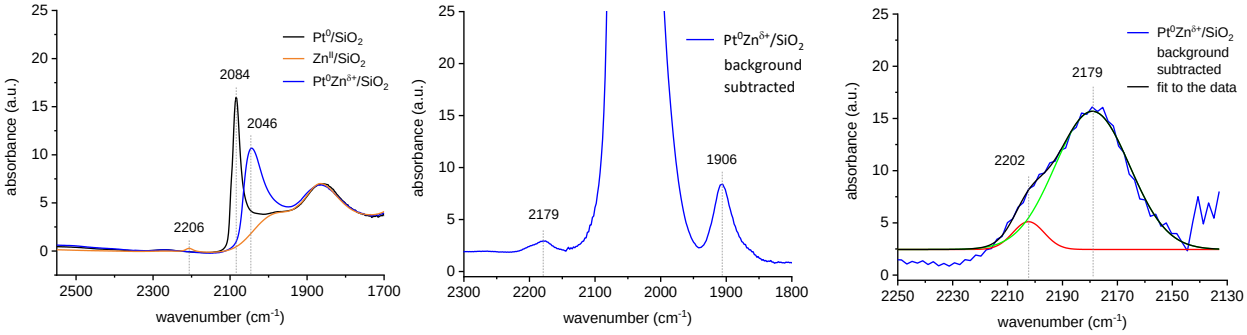

Figure S12. Left: CO adsorption on **Pt^0/SiO_2**, **Zn^{II}/SiO_2** and **$Pt^0Zn^{\delta+}/SiO_2$**. The spectra are normalized to the υ_{SiO} vibrational frequency at 1865 cm^{-1}. Middle: Background subtracted spectrum of CO adsorption on **$Pt^0Zn^{\delta+}/SiO_2$**. Right: Two component Gaussian fit of the region at 2179 cm^{-1} of **$Pt^0Zn^{\delta+}/SiO_2$**.

Pyridine adsorption/desorption IR studies.

Self-supporting pellets (12-15 mg) of **Zn^{II}/SiO_2** and **$Pt^0Zn^{\delta+}/SiO_2$** were freshly prepared, submitted to an atmosphere of pyridine and analyzed by transmission infrared spectroscopy at 2 cm^{-1} resolution. After placing each sample under high vacuum (10^{-5} mbar), the pellet was exposed to pyridine vapor, subsequently placed under high vacuum (10^{-5} mbar) again and analyzed by transmission infrared spectroscopy. Additional pyridine desorption experiments were performed. The self-supporting pellets were analyzed at temperature intervals of 100 °C, starting at 100 °C up to 500 °C heating with a ramp of 300 °C/min between intervals. All temperatures were maintained for a minimum of 30 minutes prior to analysis by infrared spectroscopy. Assignment of vibrational bands observed during these experiments are based on previous assignments for **Zn^{II}/SiO_2** and ZnO[3,5] as well as Pt/SiO_2 and Pt{111}.[6,7] The bands in **$Pt^0Zn^{\delta+}/SiO_2$** at 1610 cm^{-1} and 1452 cm^{-1} – similar to **Zn^{II}/SiO_2** – indicate a strong Lewis acidic site on the surface shown by the distinctive shifts and the retention of the bands upon heating. The bands at 1595 cm^{-1} and 1445 cm^{-1} most probably correspond to another Lewis acidic site, superimposed with the bands of physisorbed pyridine, indicated by an initially strong decrease in intensity of the

bands upon heating in accordance with removal of weakly bound pyridine.[5] Interestingly, the **Zn^{II}/SiO_2** material does not show retention of these bands upon heating, in accordance with only one type of Lewis acidic site. The vibrational bands at 1538 cm^{-1}, 1438 cm^{-1} and 1408 cm^{-1} can be observed for **$Pt^0Zn^{\delta+}/SiO_2$** while not observable for **Zn^{II}/SiO_2**. The band at 1538 cm^{-1} is close to what is reported for pyridine interacting with adsorbed hydrogen on Pt/SiO_2[6] while the bands at 1438 cm^{-1} and 1408 cm^{-1} are similar to α-pyridyl species on Pt{111}.[7] Additionally, the absence of bands at higher than 1610 cm^{-1} indicate a low Brønsted acidity of both **Zn^{II}/SiO_2** an **$Pt^0Zn^{\delta+}/SiO_2$**.[8] Furthermore, the pyridine desorption study supports the existence of two different Lewis acidic sites on the surface of **$Pt^0Zn^{\delta+}/SiO_2$**, in accordance with the CO adsorption study.

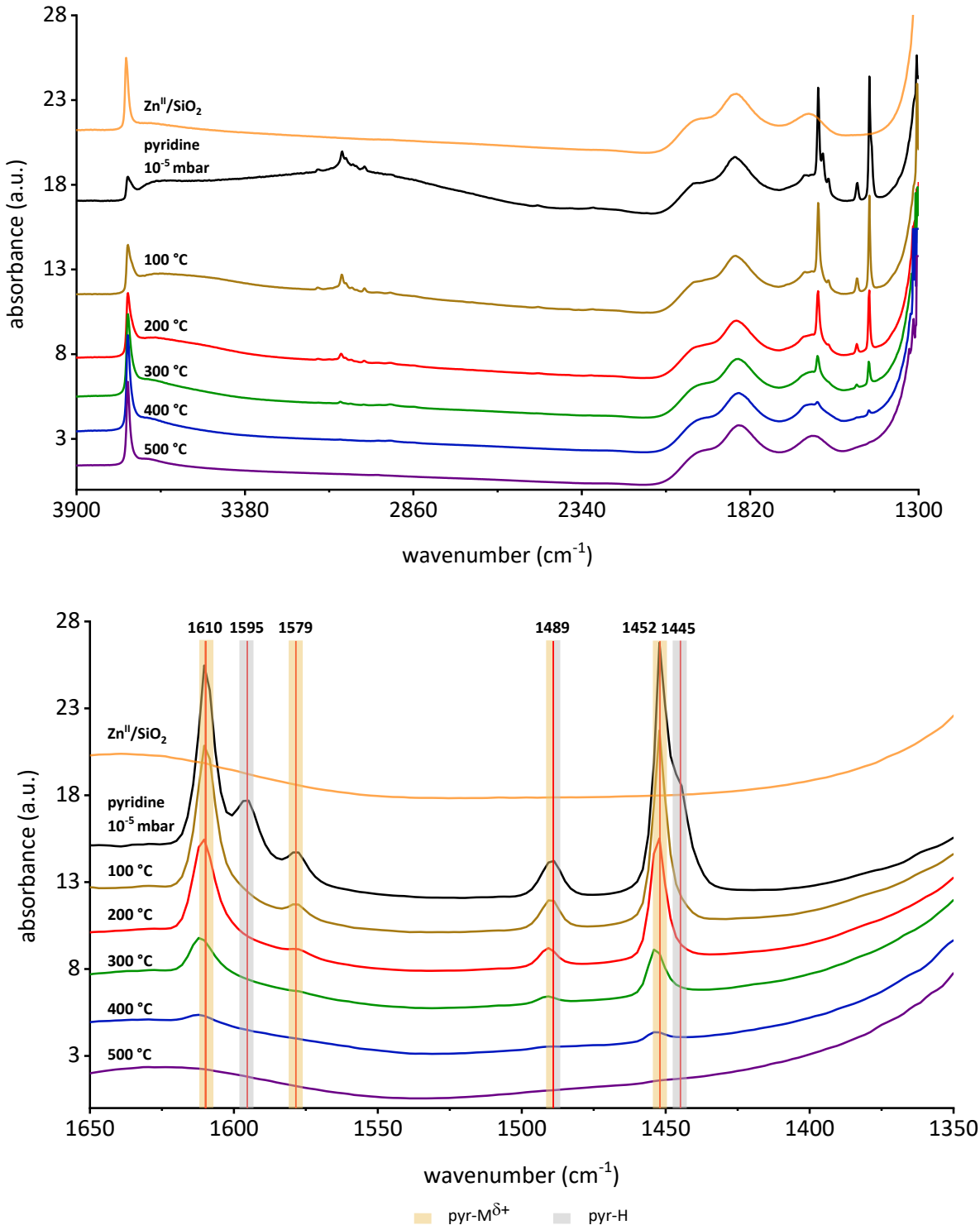

Figure S13. Upper: pyridine adsorption and desorption on **Zn^{II}/SiO_2** under high vacuum. Lower: Close-up view of the exact same spectra. All spectra are offset and normalized to the $\upsilon_{Si\text{-}O}$ vibrational frequency at 1865 cm^{-1}.

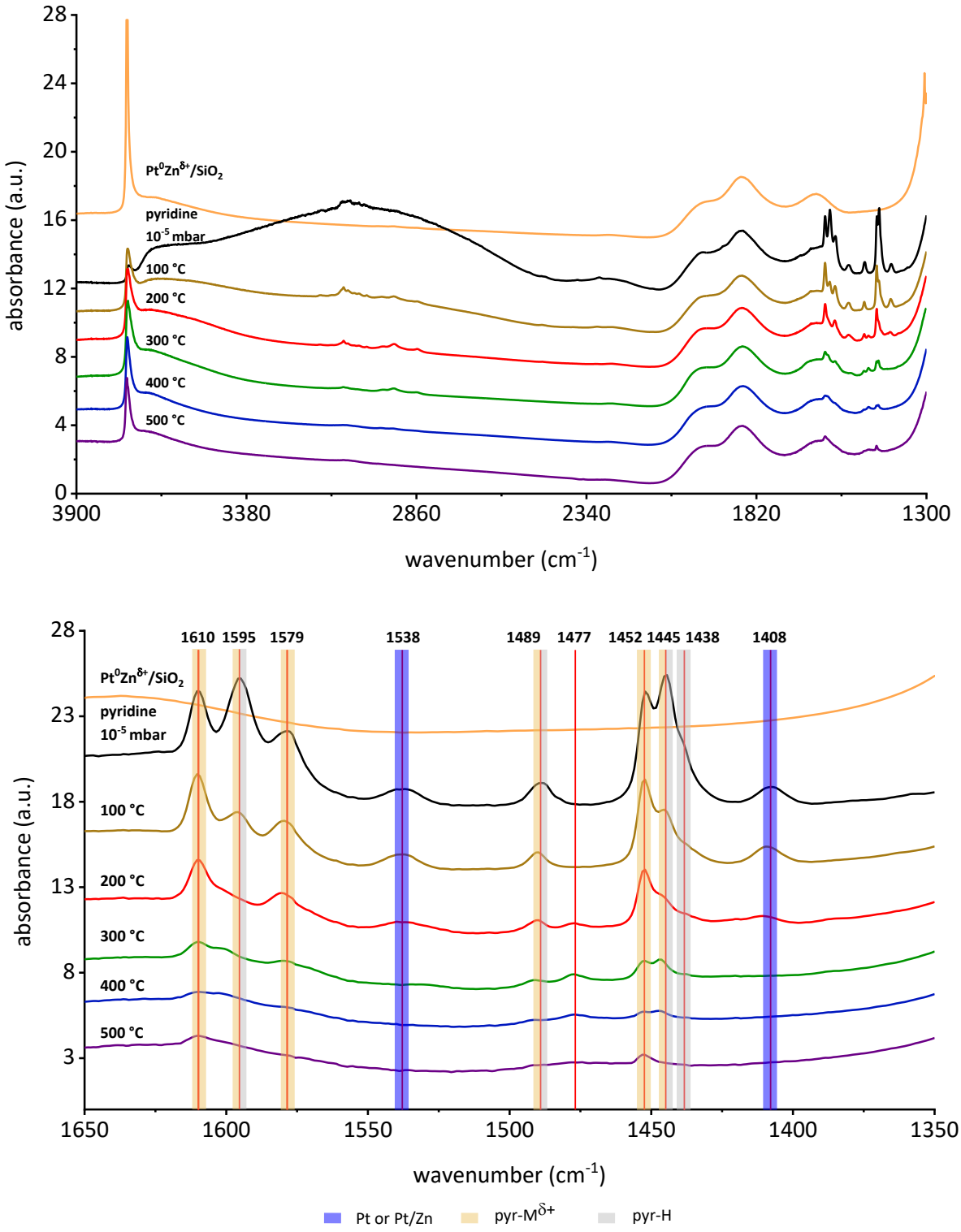

Figure S14. Upper: pyridine adsorption and desorption on **$Pt^0Zn^{\delta+}/SiO_2$** under high vacuum. Lower: Close-up view of the exact same spectra. All spectra are offset and normalized to the $\upsilon_{Si\text{-}O}$ vibrational frequency at 1865 cm^{-1}.

H_2 and CO chemisorption studies.

Chemisorption experiments were performed using a BEL JAPAN BELSORP-MAX. 150 mg to 200 mg of the samples were loaded into cells in an Ar filled and solvent-free glovebox. Pretreatment for H_2 and CO chemisorption measurements involved heating the samples at 300 °C for 3 h under dynamic vacuum. Adsorption experiments were performed at 40 °C under isothermal conditions using a circulating thermostat bath. **Pt^0/SiO_2** shows values for Q_{sat} of 1.7 mmol H_2/g_{Pt} and 2.5 mmol CO/g_{Pt} in the same temperature range while **$Pt^0Zn^{\delta+}/SiO_2$** shows lower values (vide infra).[9] Based on the particle size in **Pt^0/SiO_2** and **$Pt^0Zn^{\delta+}/SiO_2$** the trend should be reversed. This shows an inherent difference in the particle composition of the two materials, supporting alloy formation. The chemisorption curves were fitted with the following Langmuir adsorption isotherms:

$$Q_{H_2}(P) = Q_{H_2 sat} \cdot \frac{\sqrt{K_{H_2}\frac{p}{p_0}}}{1+\sqrt{K_{H_2}\frac{p}{p_0}}} \qquad \text{or} \qquad Q_{CO}(P) = Q_{CO\ sat} \cdot \frac{K_{CO}\frac{p}{p_0}}{K_{CO}\frac{p}{p_0}}$$

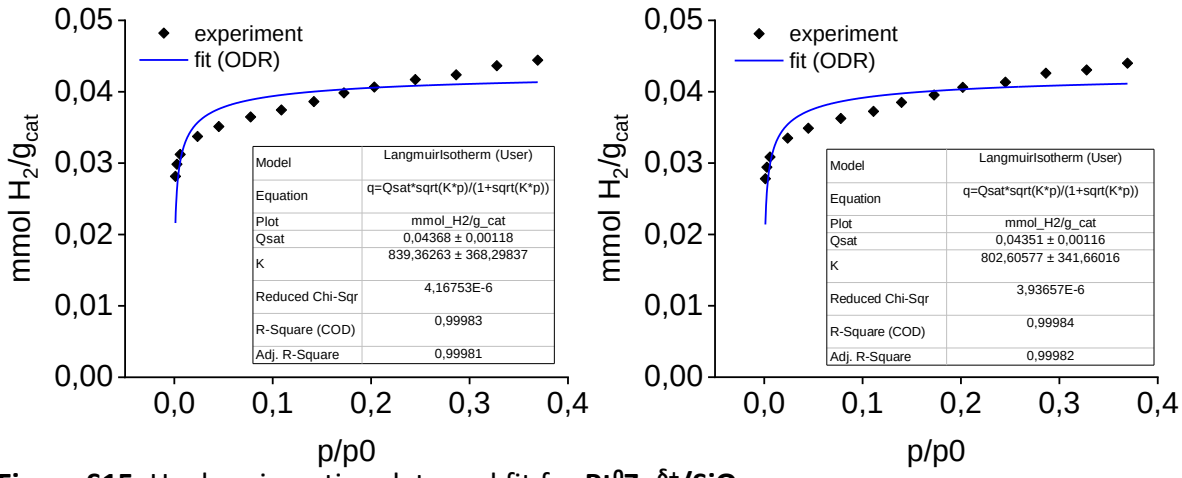

Figure S15. H_2 chemisorption data and fit for **$Pt^0Zn^{\delta+}/SiO_2$**.

Table S1. H_2 chemisorption data for **$Pt^0Zn^{\delta+}/SiO_2$**.

	1st	2nd	Avg.
$Q_{H_2 sat}\left(\frac{mmol\ H_2}{g_{Pt}}\right)$	1.450	1.456	1.45

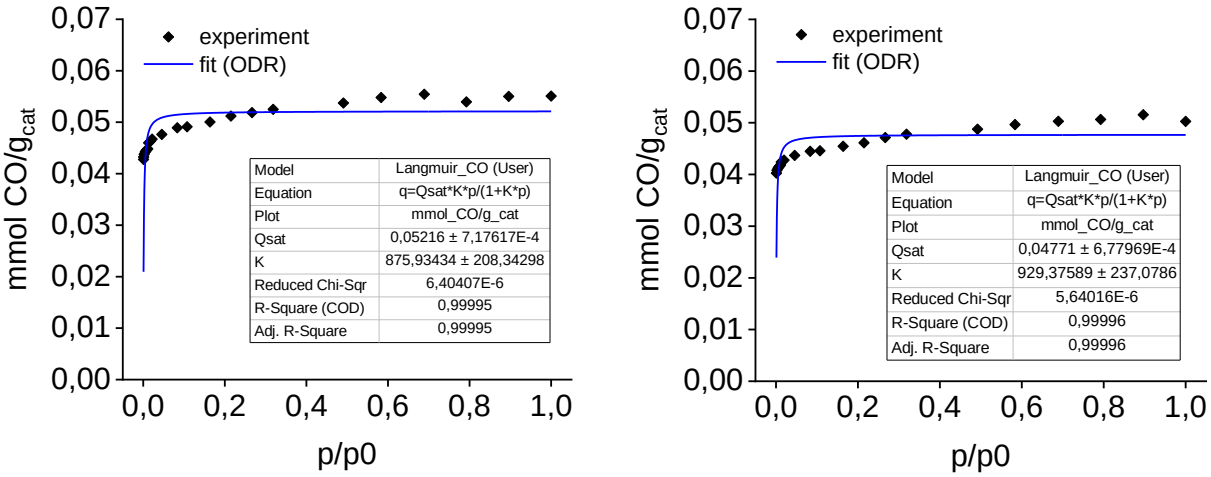

Figure S16. CO chemisorption data and fit for **$Pt^0Zn^{\delta+}/SiO_2$**.

Table S2. CO chemisorption data for **$Pt^0Zn^{\delta+}/SiO_2$**.

	1st	2nd	Avg.
$Q_{CO\ sat}\left(\frac{mmol\ CO}{g_{Pt}}\right)$	1.739	1.590	1.66

XPS studies.

XPS data were obtained using a Kratos Axis Ultra DLD spectrometer with monochromic Al Kα radiation (1486.6 eV) at pass energy (PE) of 20 and 160eV for high-resolution and survey spectra, respectively. A commercial Kratos charge neutralizer was used to avoid non-homogeneous electric charge of non-conducting powder and to achieve better resolution. Typical instrument resolution for PE of 20eV is ~0.35 eV. Binding energy (BE) values refer to the Fermi edge and the energy scale was calibrated using Au $4f_{7/2}$ at 84.0 eV and Cu $2p_{3/2}$ at 932.67 eV. Samples, powder, were placed on a stainless-steel sample holder bar using a double-sided sticking Cu tape. Samples were mounted in a Ar-filled glove box attached to the XPS instrument avoiding any contact with air. XPS data were analyzed with CasaXPS software (www.casaxps.com). Prior to data analysis, the Si $2p_{3/2}$ peak was set to a binding energy of 103.5 eV to correct for charge on each sample. Curve-fitting was performed following a Shirley background subtraction using Gaussian-Lorentzian peak shapes.

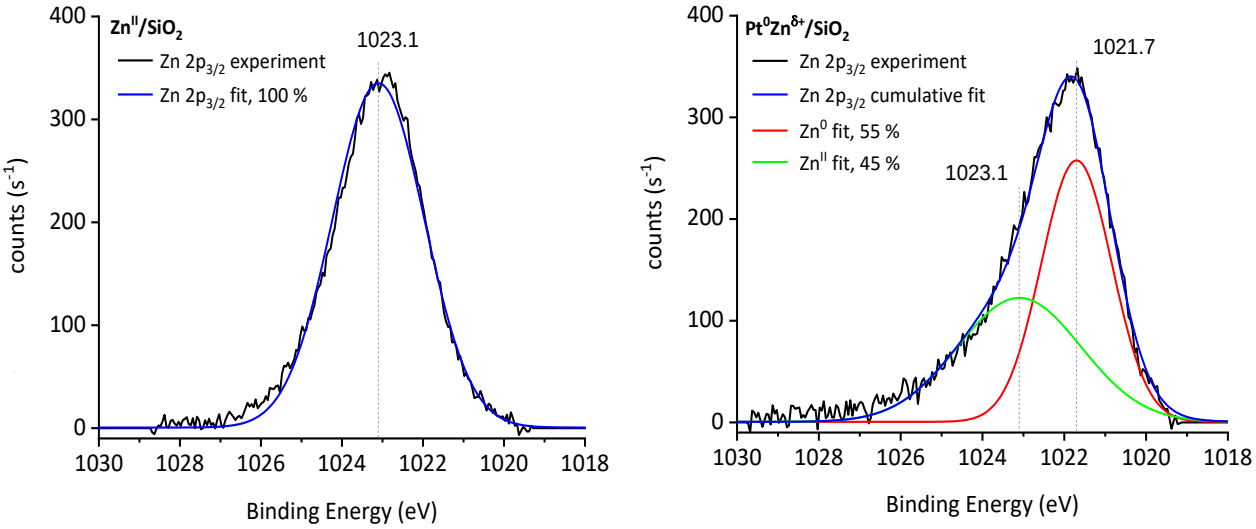

Figure S17. High resolution Zn $2p_{3/2}$ XPS spectra of **Zn^{II}/SiO_2** (left) and **$Pt^0Zn^{\delta+}/SiO_2$** (right).

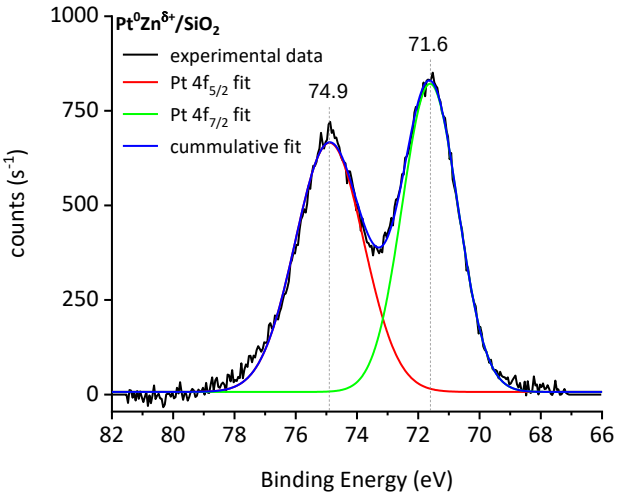

Figure S18. High resolution Pt 4*f* XPS spectrum of **$Pt^0Zn^{\delta+}/SiO_2$**.

XAS studies.

XAS measurements were carried out at the Zn K-edge and Pt L_3-edge at the SuperXAS beamline at SLS (PSI, Villigen, Switzerland). The storage ring was operated at 2.4 GeV in top-up mode with a ring current of around 400 mA. The incident photon beam provided by a 2.9 T superbend magnet was selected by a Si(111) quick-EXAFS monochromator and the rejection of higher harmonics and focusing were achieved by a rhodium-coated collimating mirror at 2.5 mrad and a rhodium-coated torroidal mirror at 2.5 mrad. The beamsize on the sample was 100 x 100 µm. During measurements, the monochromator was rotating with 1 Hz frequency in 2 deg angular range and X-ray absorption spectra were collected in transmission mode using ionization chambers specially developed for quick data collection with 1 MHz frequency.[10] The spectra were collected for 3 min and averaged. The beamline energy was calibrated with either the Zn reference foil to the Zn K-edge position at 9659.0 eV or the Pt reference foil to the Pt L_3-edge position at 11564.0 eV, respectively. To avoid contact with air, all samples were sealed in a glovebox. For ex situ samples, pressed pellets (with optimized thickness for transmission

detection) were placed in two aluminized plastic bags (Polyaniline (15 µm), polyethylene (15 µm), Al (12 µm), polyethylene (75 µm) from Gruber-Folien GmbH & Co. KG, Straubing, Germany) using an impulse sealer inside a glovebox; one sealing layer was removed immediately before the measurements. For *in-situ* measurements, catalyst beds of appropriate mass were supported with quartz wool in 3 mm quartz capillaries. Gas flow and composition were controlled using Bronkhorst mass flow controllers and a back-pressure regulator. Flow rates during H_2 reduction were maintained at 10 ml/min with a pressure of 1 atmosphere. PDH studies were performed at flow rates of 50 ml/min (20% C_3H_8/Ar) with a pressure of 1 atmosphere. Ar, H_2 and propane were purified by passing through a column with molecular sieves and Q5 catalyst prior to introduction to the XAS quartz cell. Data processing was done by standard procedures using the ProXASGui software developed at the SuperXAS beamline, PSI, Villigen. The program package Demeter was used for data analysis.[11] $S0^2$ values for the Zn K-edge and Pt L_3-edge were obtained by fitting Pt and Zn foil, respectively. Coordination numbers were fixed for both cases.

Zn K edge.

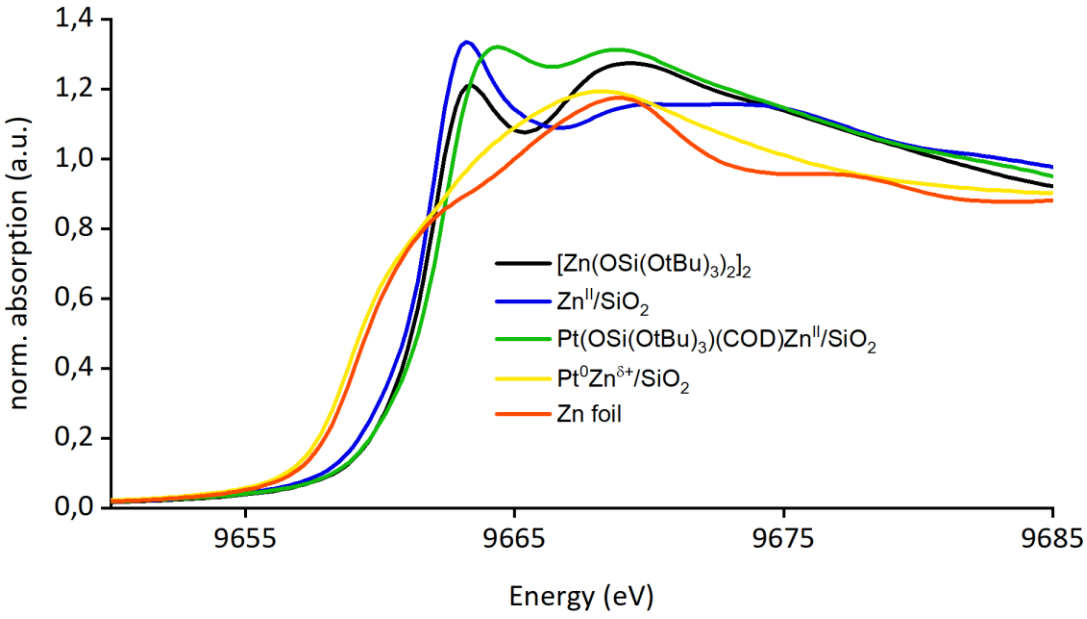

Figure S19. XANES spectra at the Zn K edge of **$[Zn(OSi(OtBu)_3)_2]_2$**, **Zn^{II}/SiO_2**, **$Pt(OSi(OtBu)_3)(COD)Zn^{II}/SiO_2$**, **$Pt^0Zn^{\delta+}/SiO_2$** and Zn foil.

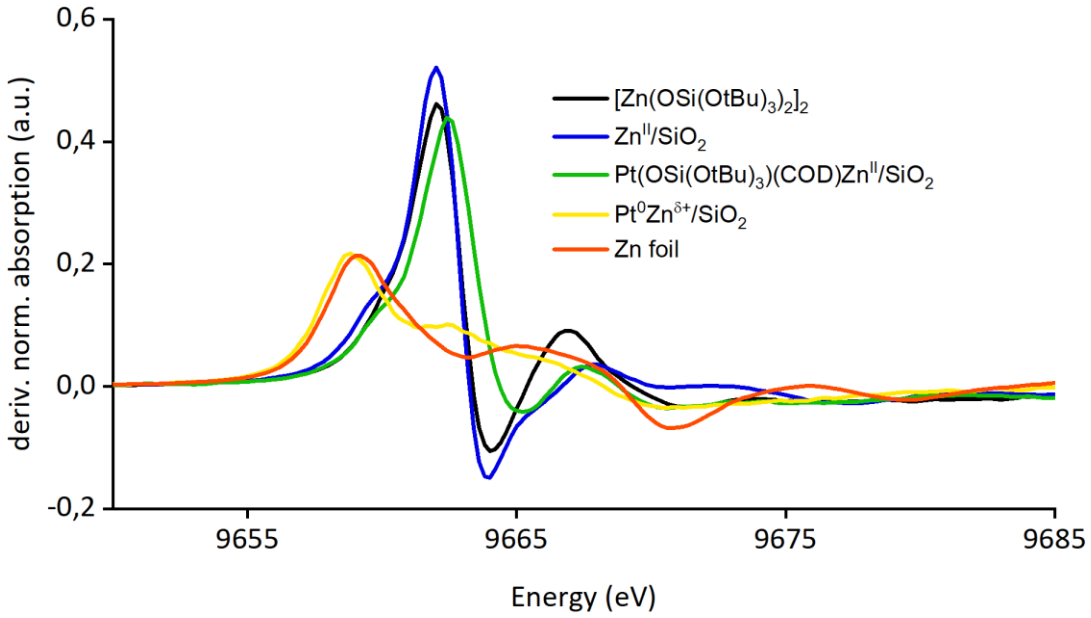

Figure S20. First derivative of XANES spectra at the Zn K edge of **$[Zn(OSi(OtBu)_3)_2]_2$**, **Zn^{II}/SiO_2**, **$Pt(OSi(OtBu)_3)_2(COD)Zn^{II}/SiO_2$**, **$Pt^0Zn^{\delta+}/SiO_2$** and Zn foil.

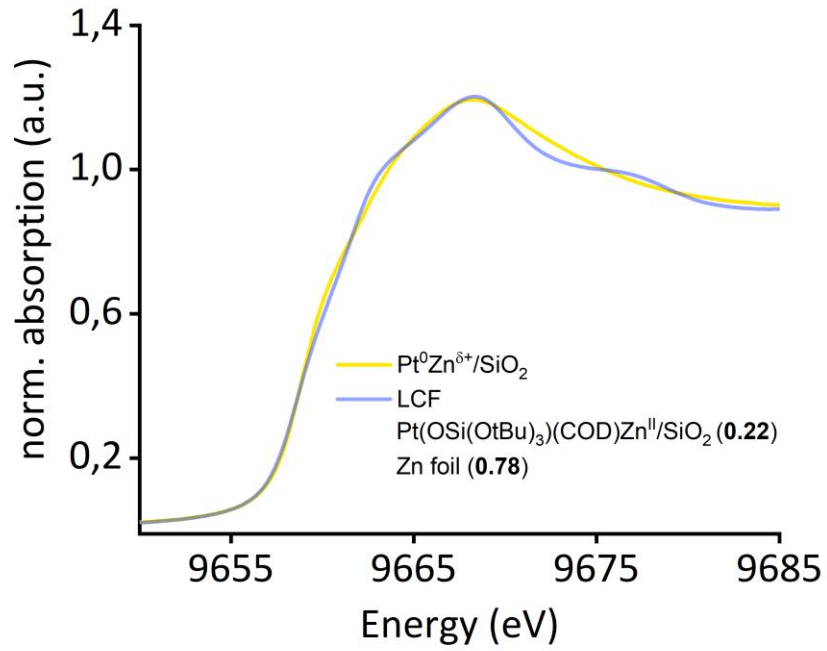

Figure S21. $Pt(OSi(OtBu)_3)_2(COD)Zn^{II}/SiO_2$ and Zn foil linear combination fit of **$Pt^0Zn^{\delta+}/SiO_2$**.

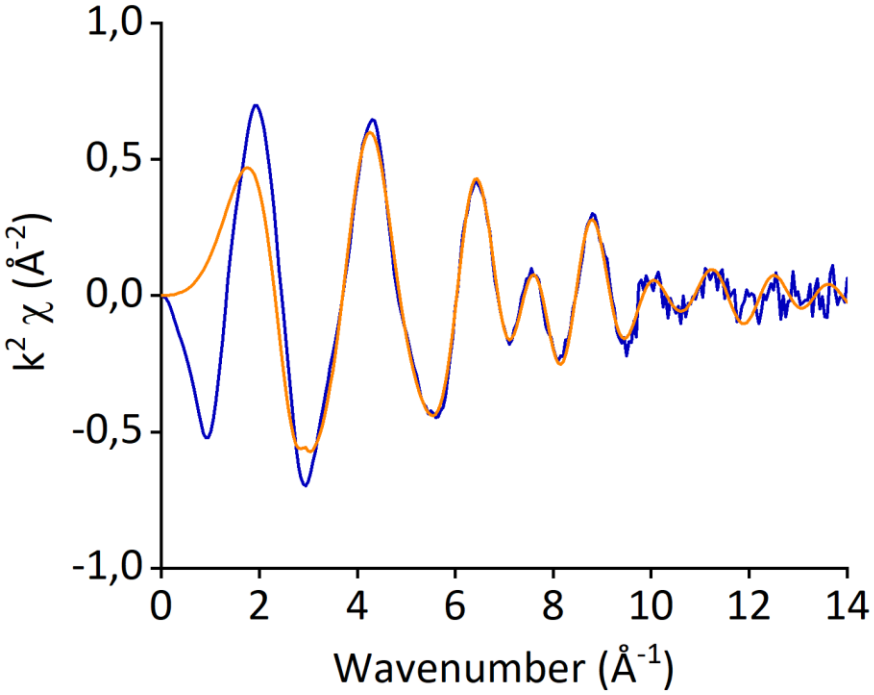

Figure S22. EXAFS data and fit for **[Zn(OSi(OtBu)$_3$)$_2$]$_2$** in *k*-space at the Zn K edge.

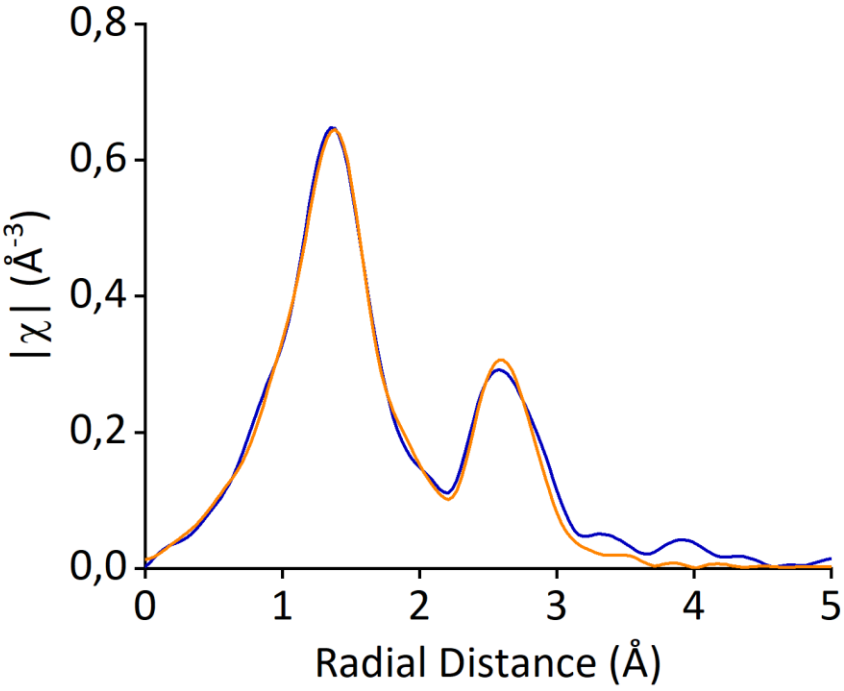

Figure S23. EXAFS data and fit for **[Zn(OSi(OtBu)$_3$)$_2$]$_2$** in *R*-space at the Zn K edge.

Table S3. EXAFS fit parameters for **$[Zn(OSi(OtBu)_3)_2]_2$**. $S0^2$=0.85; k range 3-12 Å; R range 1-3.5; k weight 2. Numbers without errors were fixed in the EXAFS fits.

Path	N	R, Å	σ^2, Å^2	ΔE0, eV
Zn-O	**3**	**1.86 +/- 0.02**	**0.009 +/- 0.002**	**-1.3 +/- 3.7**
Zn-O	**1**	**2.03 +/- 0.07**	**0.010 +/- 0.009**	
Zn-Si	**1**	**2.69 +/- 0.05**	**0.016 +/- 0.007**	
Zn-Zn	**1**	**2.90 +/- 0.02**	**0.005 +/- 0.001**	
Zn-Si	**1**	**3.50 +/- 0.04**	**0.006 +/- 0.004**	

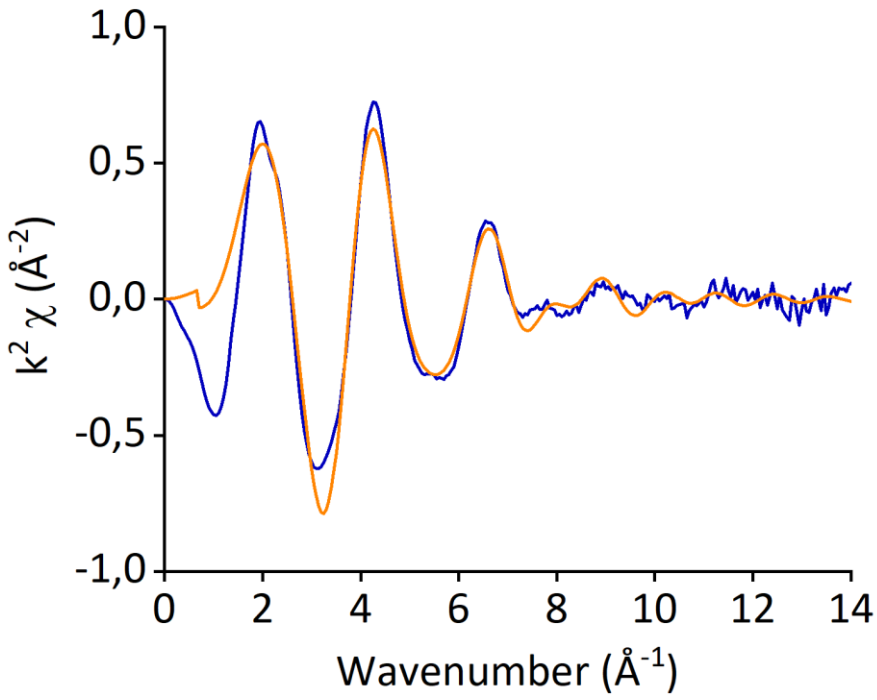

Figure S24. EXAFS data and fit for **Zn^{II}/SiO_2** in *k*-space at the Zn K edge. The inclusion of a Zn-Zn path results in a worse fit.

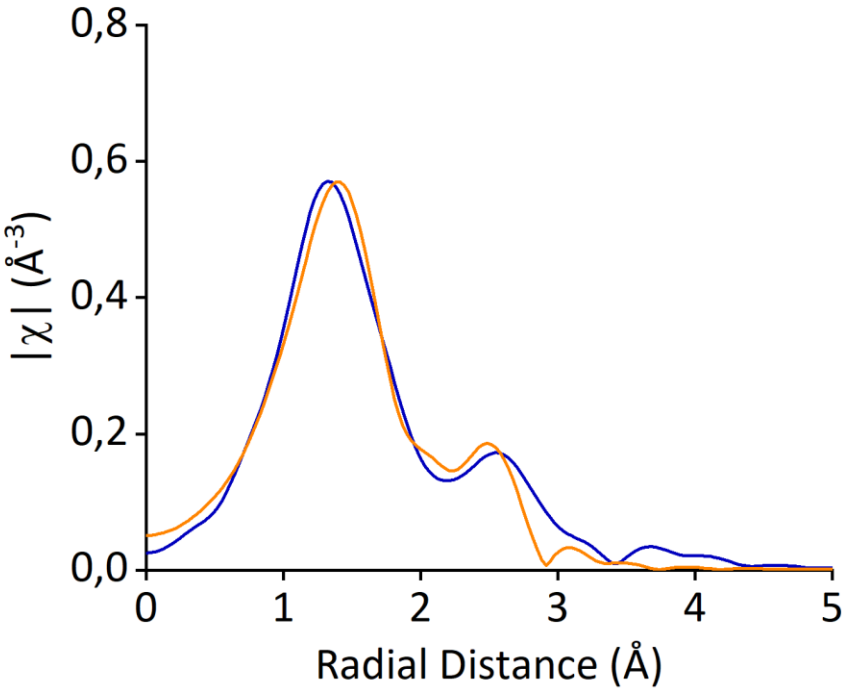

Figure S25. EXAFS data and fit for **Zn^{II}/SiO_2** in *R*-space at the Zn K edge. The inclusion of a Zn-Zn path corresponding to the dimer structure results in a worse fit.

Table S4. EXAFS fit parameters for **Zn^{II}/SiO_2**. $S0^2$=0.85; k range 3-12 Å; R range 1-3 Å; k weight 2.

Path	**N**	**R, Å**	**σ^2, Å^2**	**ΔE0, eV**
Zn-O	**3.5 +/- 0.9**	**1.88+/- 0.02**	**0.016 +/- 0.004**	**1.6 +/- 2.2**
Zn-Si	**0.7 +/- 0.6**	**3.07 +/- 0.04**	**0.005 +/- 0.008**	

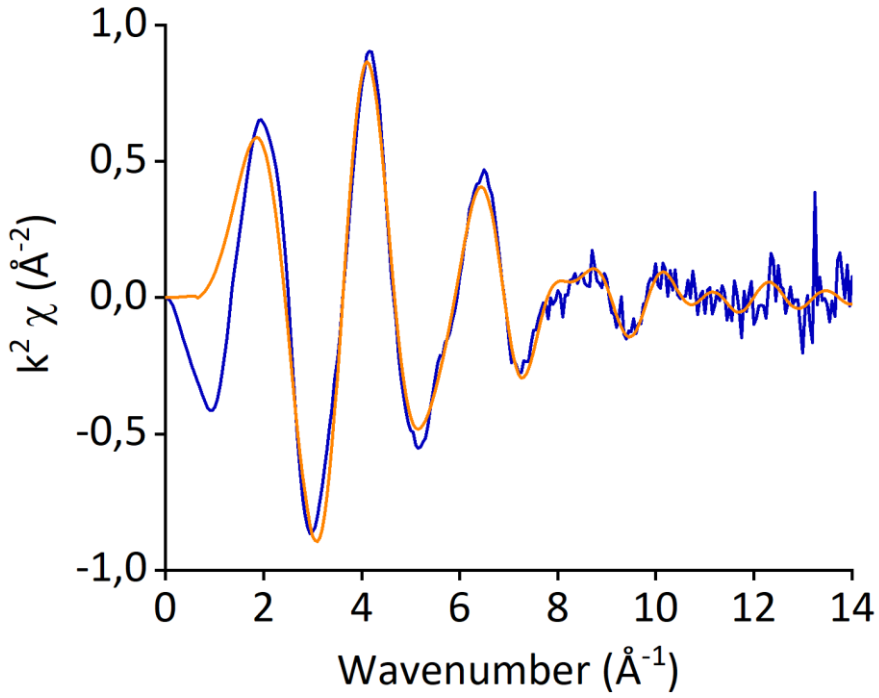

Figure S26. EXAFS data and fit for **Pt(OSi(OtBu)$_3$)(COD)Zn^{II}/SiO$_2$** in *k*-space at the Zn K edge. The inclusion of a Zn-Zn path corresponding to the dimer structure results in a worse fit.

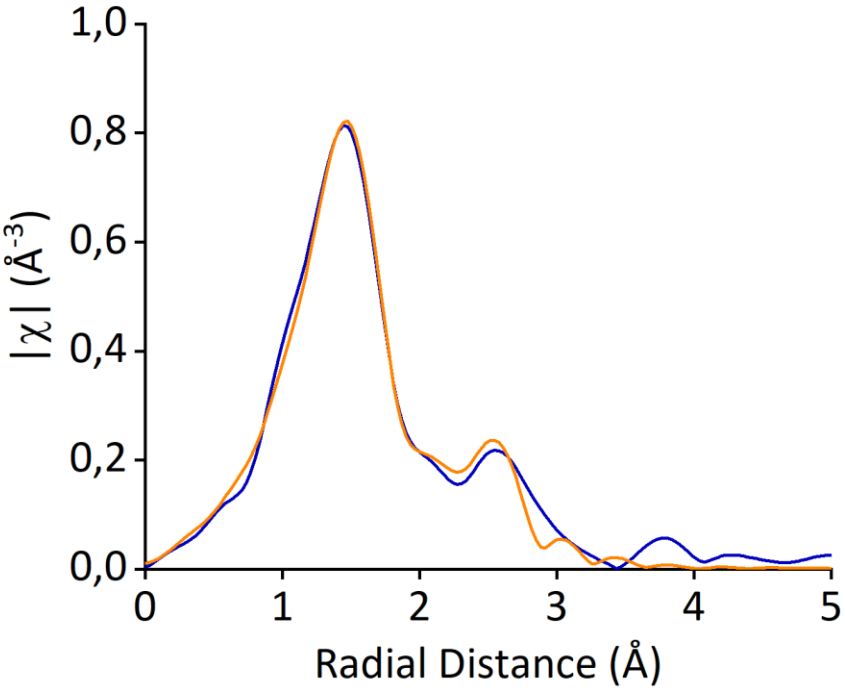

Figure S27. EXAFS data and fit for **Pt(OSi(OtBu)$_3$)(COD)Zn^{II}/SiO$_2$** in *R*-space at the Zn K edge. The inclusion of a Zn-Zn path corresponding to the dimer structure results in a worse fit.

Table S5. EXAFS fit parameters for **Pt(OSi(OtBu)$_3$)(COD)Zn^{II}/SiO$_2$** . S0^2=0.85; k range 3-11 Å; R range 1-3 Å; k weight 2.

Path	N	R, Å	σ^2, Å^2	ΔE0, eV
Zn-O	3.8 +/- 0.5	1.94 +/- 0.01	0.011 +/- 0.002	1.4 +/- 1.2
Zn-Si	0.7 +/- 0.4	3.09+/- 0.02	0.002 +/- 0.004	

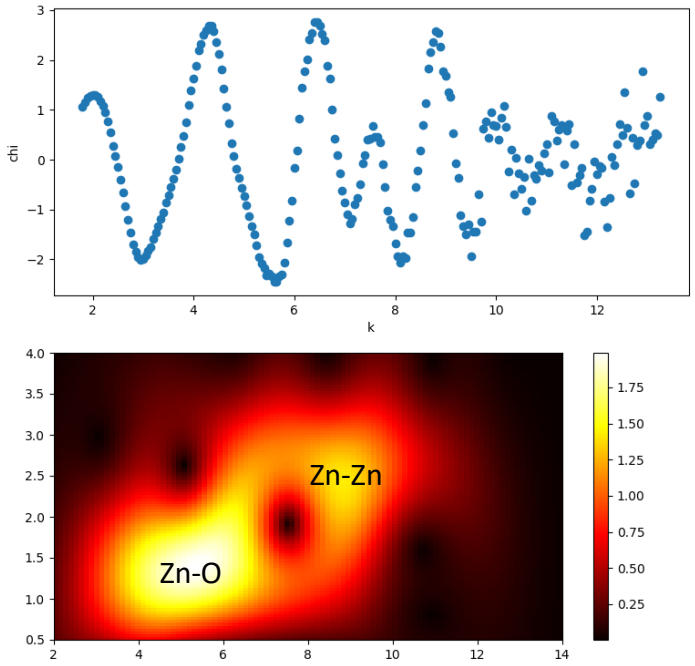

Figure S28. Wavelet transformation analysis of Zn K edge EXAFS data for **[Zn(OSi(OtBu)$_3$)$_2$]$_2$**.

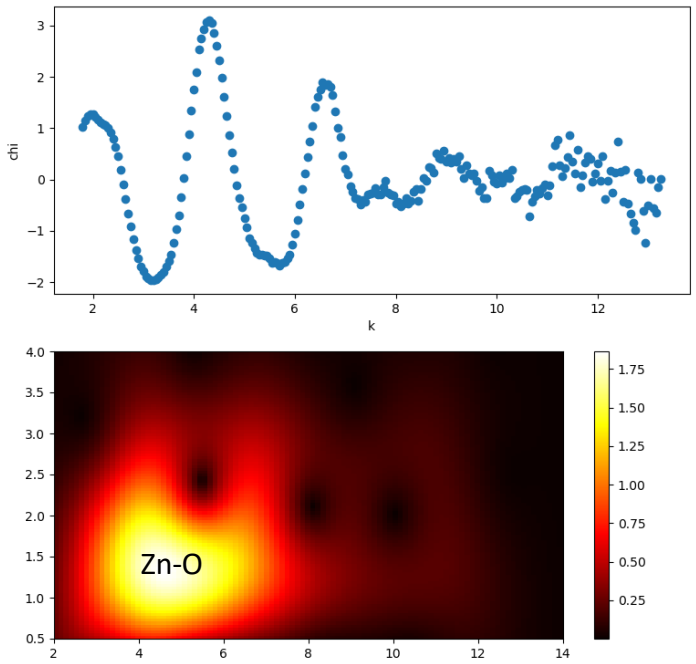

Figure S29. Wavelet transformation analysis of Zn K edge EXAFS data for **Zn^{II}/SiO_2**.

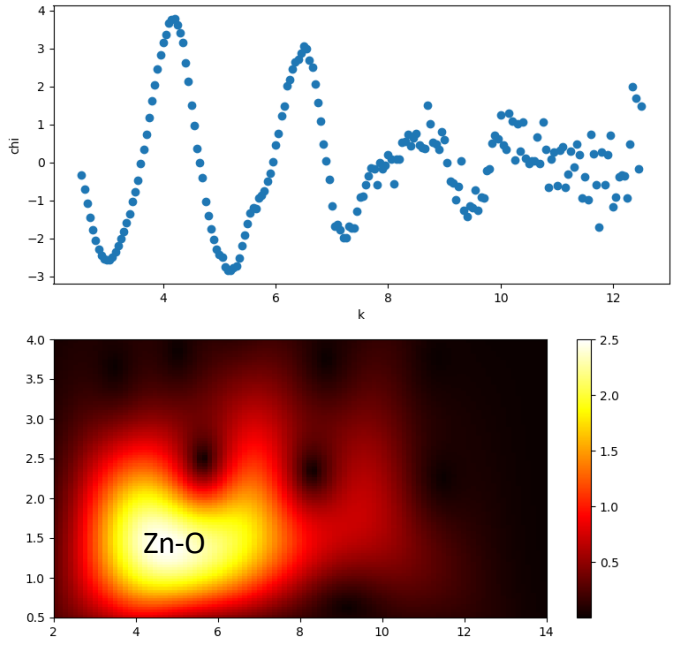

Figure S30. Wavelet transformation analysis of Zn K edge EXAFS data for **$Pt(OSi(OtBu)_3)(COD)Zn^{II}/SiO_2$**.

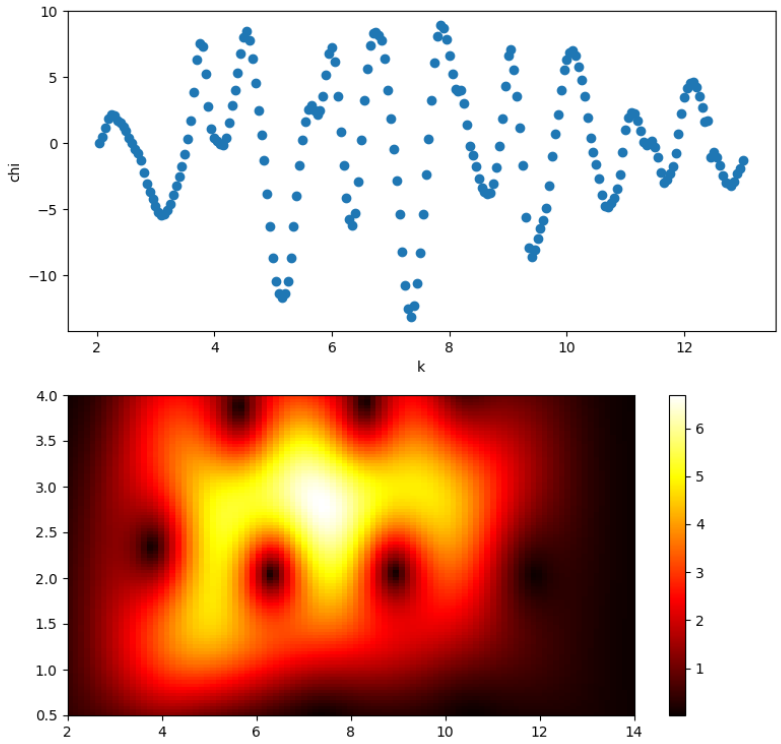

Figure S31. Wavelet transformation analysis of Zn K edge EXAFS data for **ZnO**.

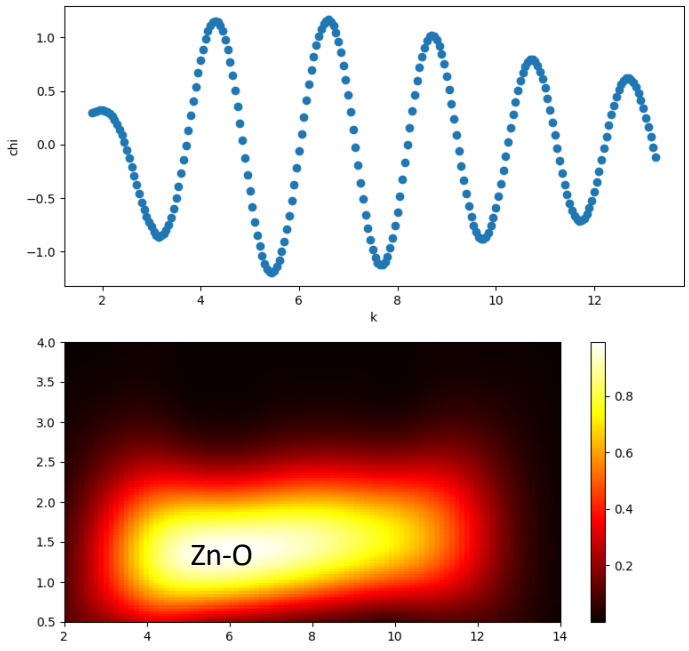

Figure S32. Wavelet transformation of simulated Zn-O path following a **$[Zn(OSi(OtBu)_3)_2]_2$** model.

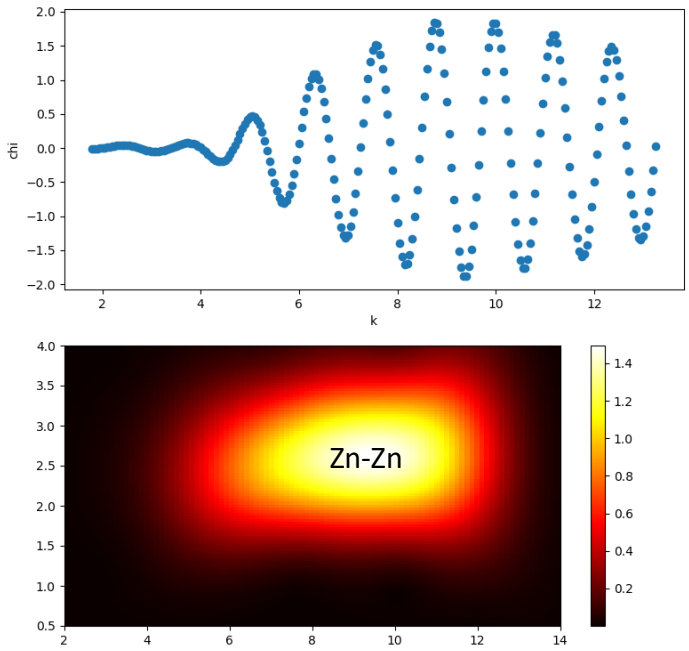

Figure S33. Wavelet transformation of simulated Zn-Zn path following a **$[Zn(OSi(OtBu)_3)_2]_2$** model.

Pt L_3 edge.

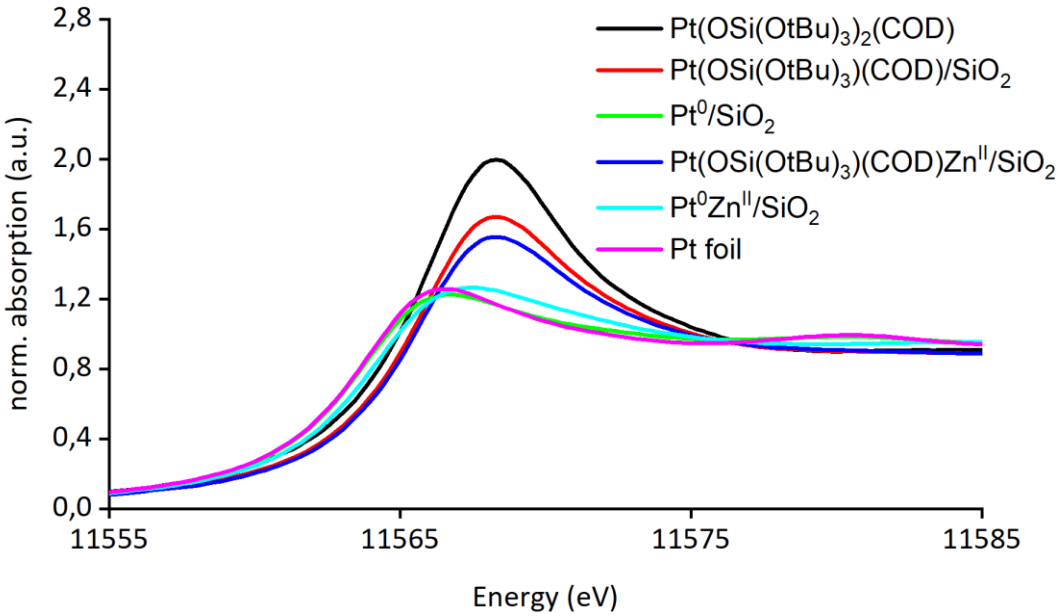

Figure S34. XANES spectra at the Pt L_3 edge of **$Pt(OSi(OtBu)_3)_2(COD)$**, **$Pt(OSi(OtBu)_3)(COD)/SiO_2$**, **$Pt^0/SiO_2$**, **$Pt(OSi(OtBu)_3)(COD)Zn^{II}/SiO_2$**, **$Pt^0Zn^{\delta+}/SiO_2$** and Pt foil.

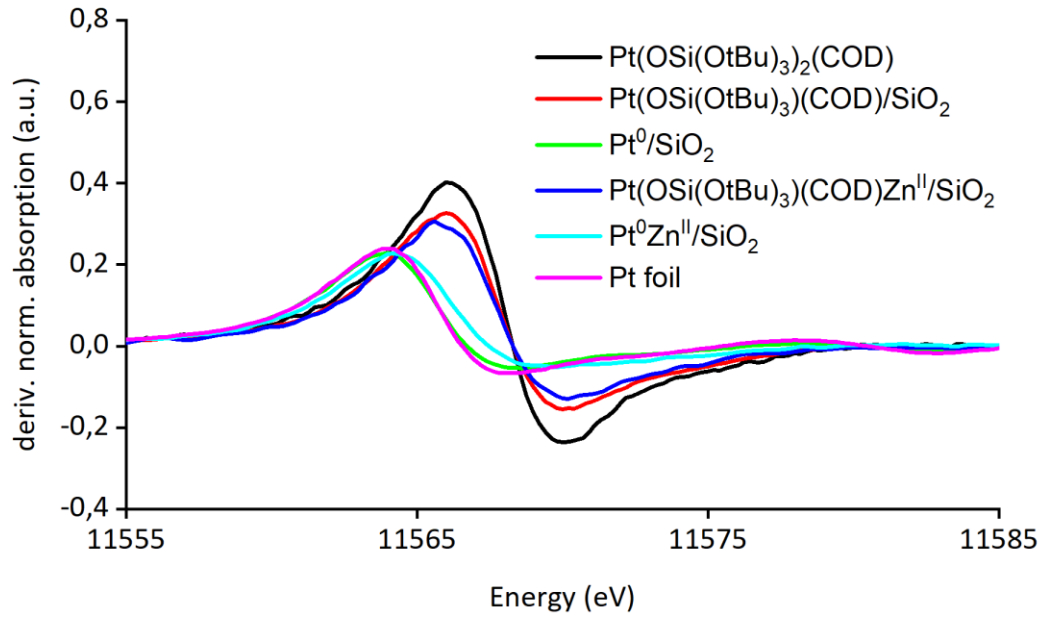

Figure S35. First derivative of XANES spectra at the Pt L_3 edge of **$Pt(OSi(OtBu)_3)_2(COD)$**, **$Pt(OSi(OtBu)_3)(COD)/SiO_2$**, **$Pt^0/SiO_2$**, **$Pt(OSi(OtBu)_3)(COD)Zn^{II}/SiO_2$**, **$Pt^0Zn^{\delta+}/SiO_2$** and Pt foil.

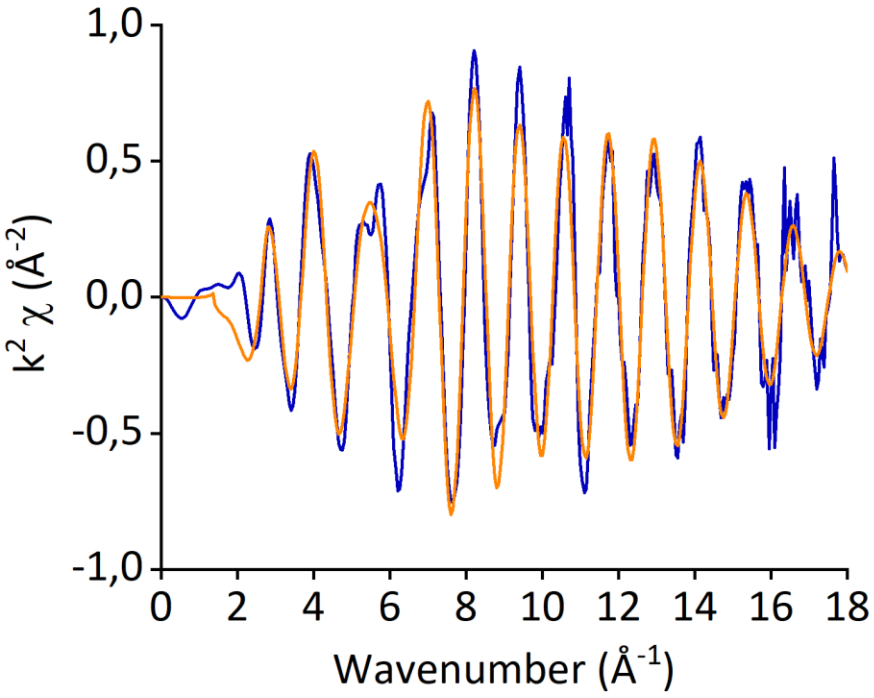

Figure S36. EXAFS data and fit for **Pt^0/SiO_2** in *k*-space at the Pt L_3 edge.

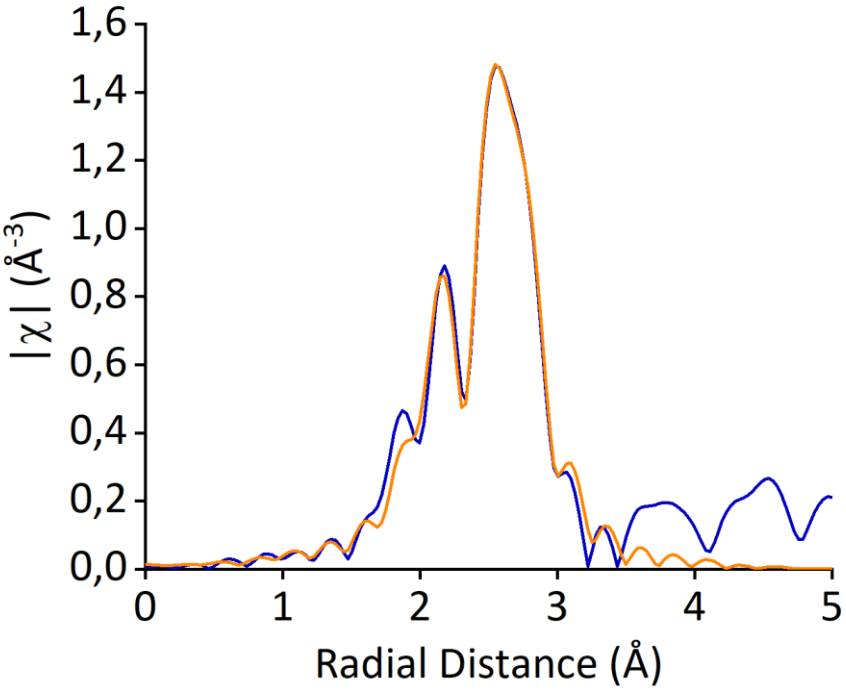

Figure S37. EXAFS data and fit for **Pt^0/SiO_2** in *R*-space at the Pt L_3 edge.

Table S6. EXAFS fit parameters for **Pt^0/SiO_2**. $S0^2$=0.84; k range 3-16 Å; R range 1-3 Å; k weight 2.

Path	N	R, Å	σ^2, Å^2	ΔE0, eV
Pt-Pt	9.1 +/- 0.4	2.747 +/- 0.002	0.0058 +/- 0.0002	7.2 +/- 0.5

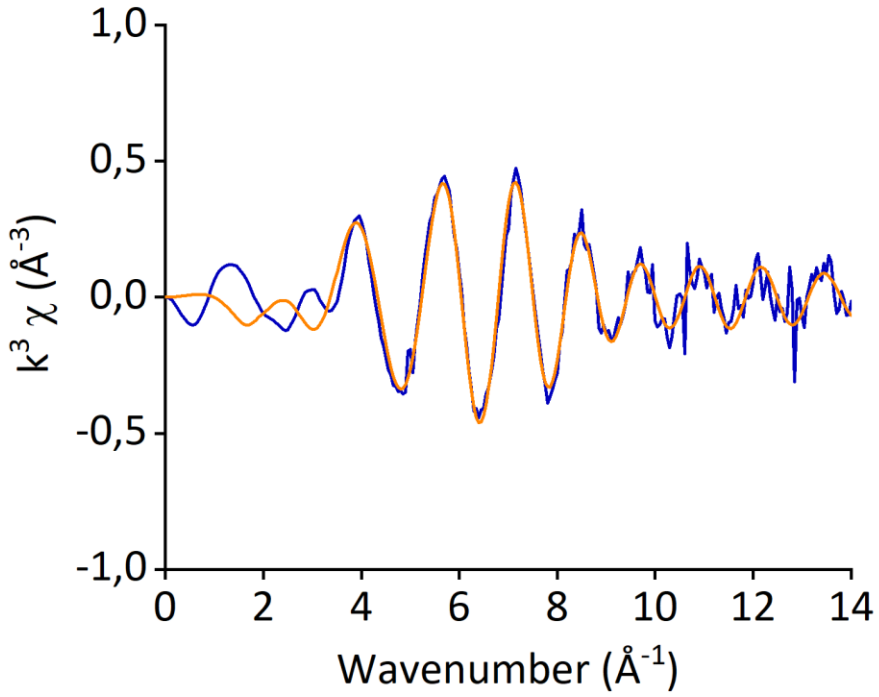

Figure S38. EXAFS data and fit for **$Pt^0Zn^{\delta+}/SiO_2$** in *k*-space at the Pt L_3 edge.

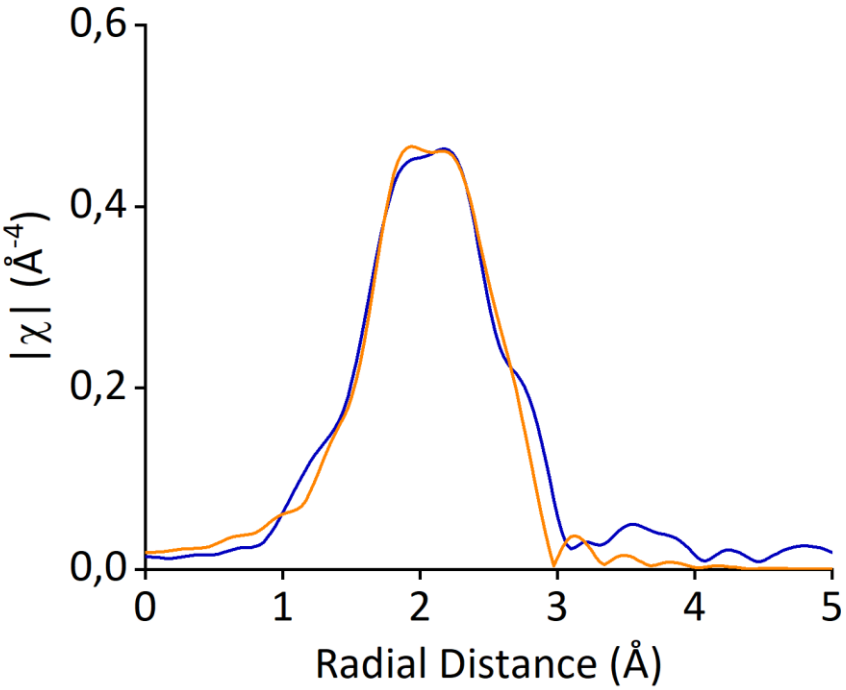

Figure S39. EXAFS data and fit for **$Pt^0Zn^{\delta+}/SiO_2$** in *R*-space at the Pt L_3 edge.

Table S7. EXAFS fit parameters for **$Pt^0Zn^{\delta+}/SiO_2$**. $S0^2$=0.84; k range 3-12 Å; R range 1-3 Å; k weight 3.

Path	N	R, Å	σ^2, Å^2	ΔE0, eV
Pt-Zn	6.7 +/- 2.4	2.48 +/- 0.03	0.022 +/- 0.004	-8.4 +/- 2.7
Pt-Pt	3.1 +/- 1.4	2.62 +/- 0.01	0.008 +/- 0.002	

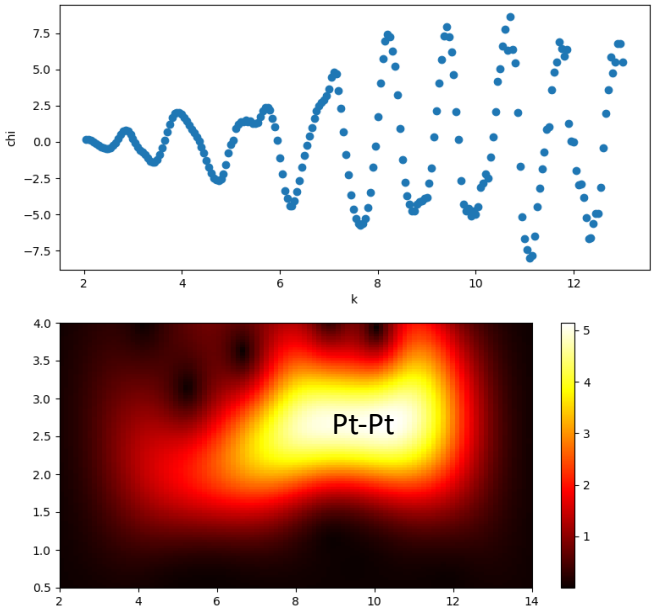

Figure S40. Wavelet transformation analysis of Pt L_3 edge EXAFS data for **Pt^0/SiO_2**.

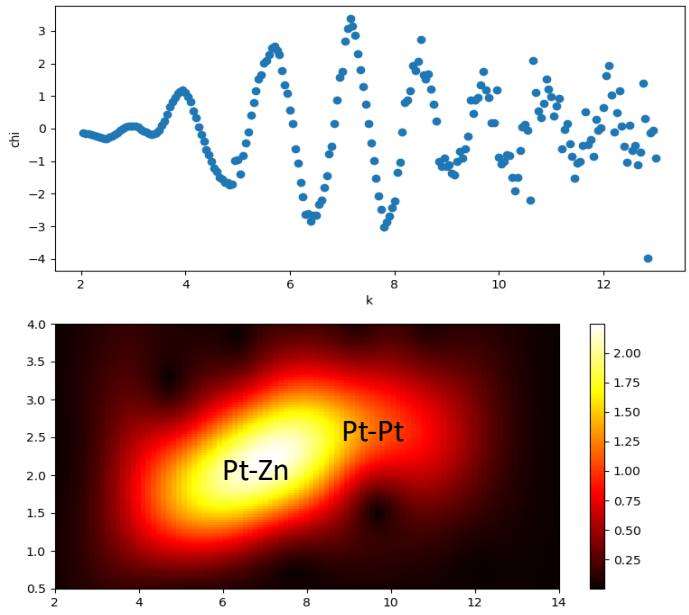

Figure S41. Wavelet transformation analysis of Pt L_3 edge EXAFS data for **$Pt^0Zn^{\delta+}/SiO_2$**.

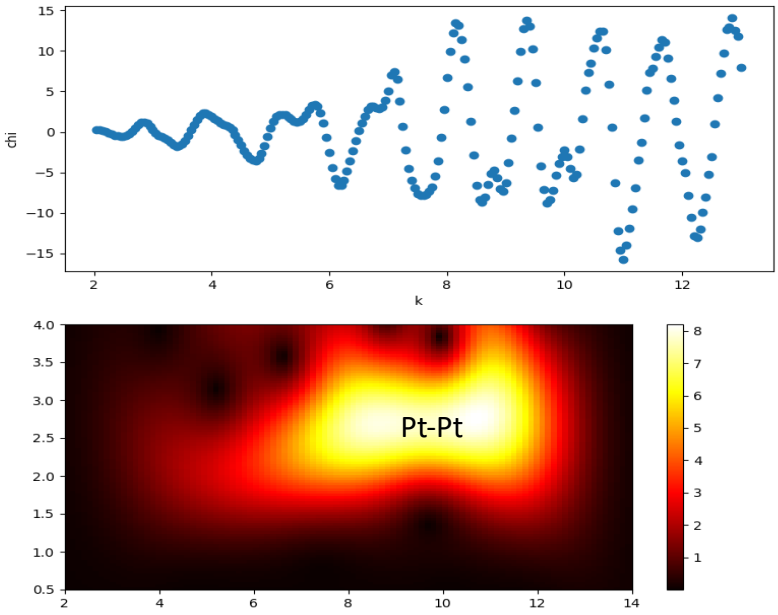

Figure S42. Wavelet transformation analysis of Pt L_3 edge EXAFS data for Pt foil.

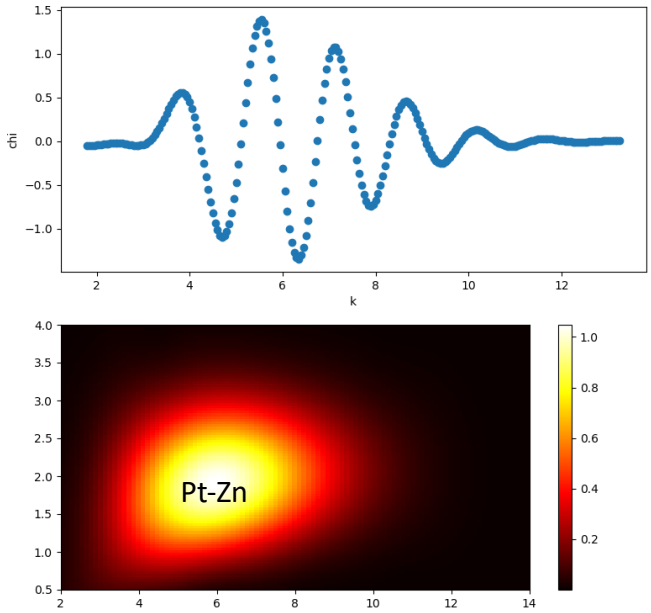

Figure S43. Wavelet transformation of simulated Pt-Zn path following a Pt_1Zn_1 model.[12]

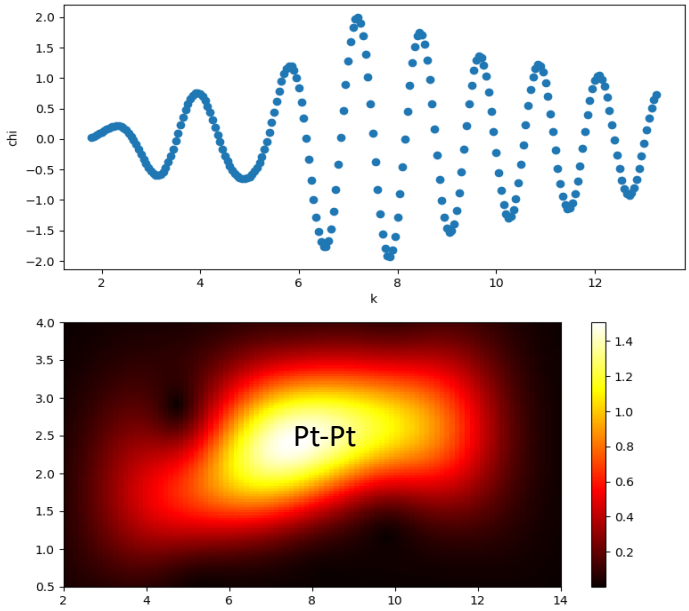

Figure S44. Wavelet transformation of simulated Pt-Pt path following a Pt_1Zn_1 model.[12]

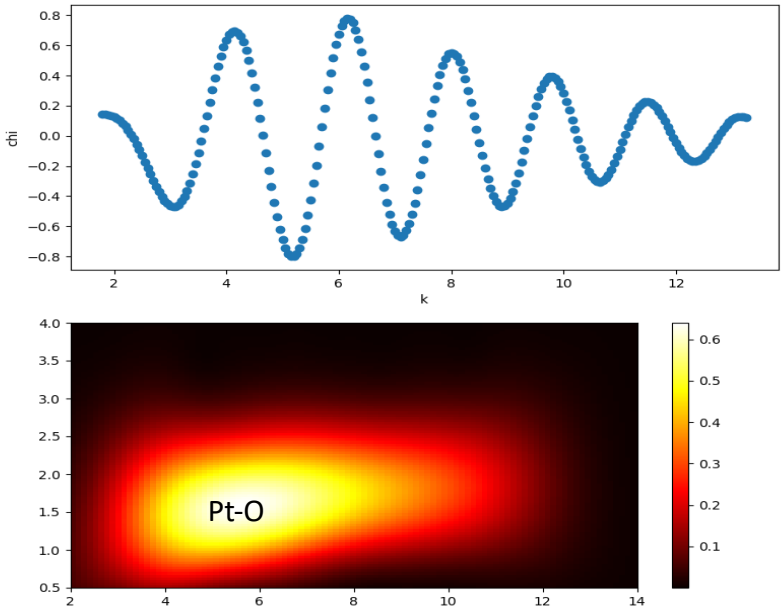

Figure S45. Wavelet transformation of simulated Pt-O path following a **$Pt(OSi(OtBu)_3)_2(COD)$** model.

In-situ XAS data.

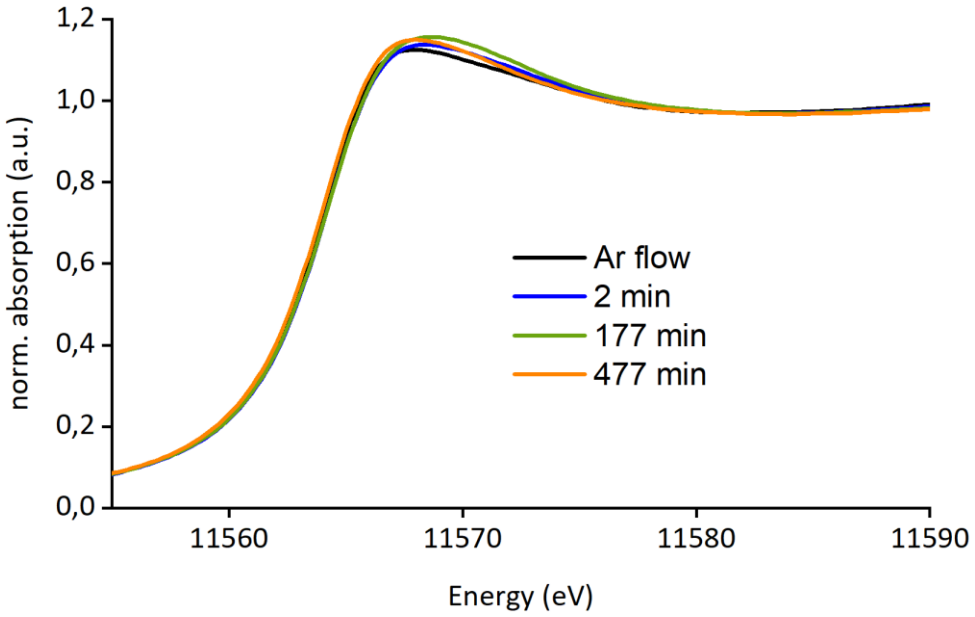

Figure S46. *In-situ* PDH XANES spectra at the Pt L_3 edge of **$Pt^0Zn^{\delta+}/SiO_2$** recorded over 8 h.

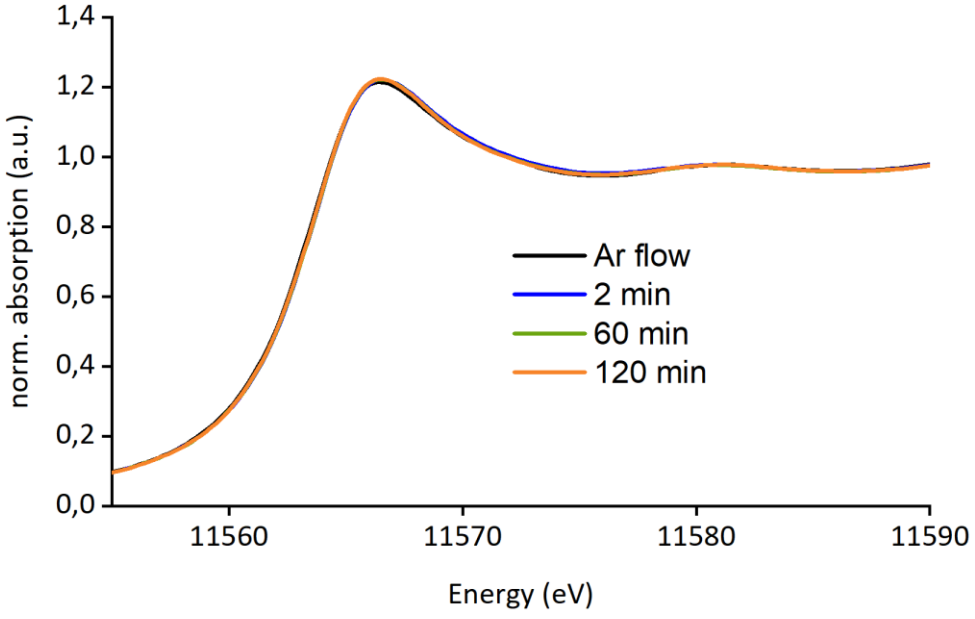

Figure S47. *In-situ* PDH XANES spectra at the Pt L_3 edge of **Pt^0/SiO_2** recorded over 2 h.

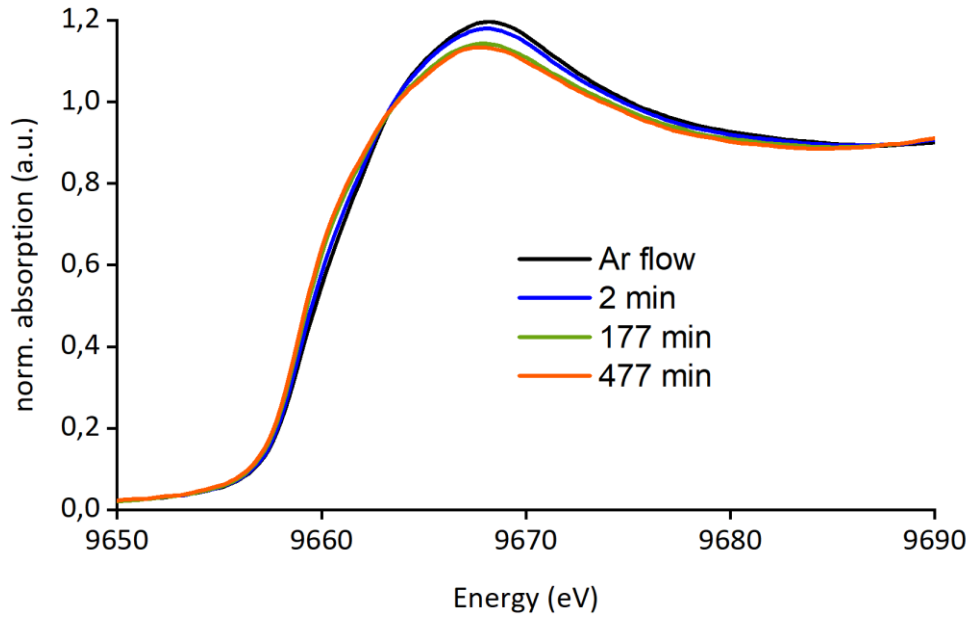

Figure S48. *In-situ* PDH XANES spectra at the Zn K edge of **$Pt^0Zn^{\delta+}/SiO_2$** recorded over 8 h.

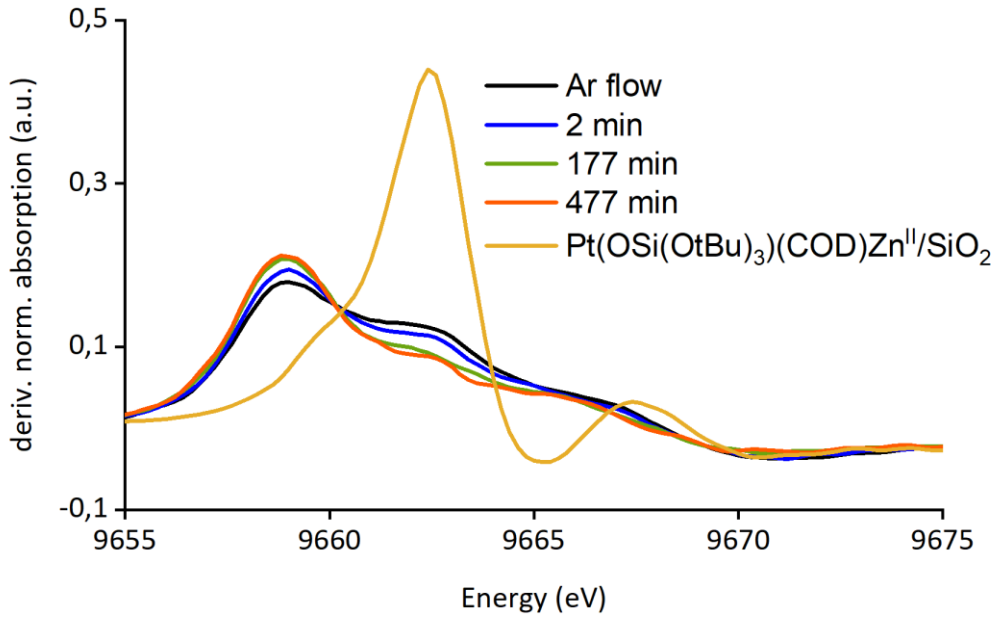

Figure S49. First derivative of *In-situ* PDH XANES spectra at the Zn K edge of **$Pt^0Zn^{\delta+}/SiO_2$** recorded over 8 h and XANES spectrum at the Zn K edge of **$Pt(OSi(OtBu)_3)(COD)Zn^{II}/SiO_2$**.

Catalytic Propane Dehydrogenation studies.

Catalytic tests were performed utilizing a stainless-steel plug-flow reactor designed by PID Engineering. Catalyst samples were loaded into a stainless-steel tubular reactor in an Ar filled glovebox. Prior to exposing the catalyst to flow conditions, a bypass was purged for 30 min with Ar (40 mL/min). The samples were then heated to 550 °C utilizing a tubular furnace under a flow of Ar (40 mL/min) and the temperature was maintained for 30 min. The gas mixture containing propane was subsequently mixed and purged through a bypass for 1 h at the desired flow rate for the reaction prior to contact with the catalyst. Reaction temperatures were maintained utilizing a thermocouple maintained in contact with the catalyst dispersed in SiC to yield a total weight of 2.5 g. The output gas composition was analyzed automatically by a GC with a flame ionization detector (FID) which was programmed to sample the gas at specific times throughout the reaction. Gases were purified by passing through a column with molecular sieves and Q5 catalyst prior to introduction to the flow reactor. Propane conversion, selectivity and the carbon balance were calculated according to following equations:

$$X_{C_3H_8} = 1 - \frac{n_{C_3H_8,out}}{n_{C_3H_8,out} + n_{C_3H_6,out} + n_{C_2H_6,out} + n_{C_2H_4,out} + n_{CH_4,out}} \quad (1)$$

$$S = \frac{n_{i,out}}{n_{i-l,out}} \quad (2)$$

$$carbon\ balance = \frac{n_{C_3H_8,in}}{n_{C_3H_8,out} + n_{C_3H_6,out} + n_{C_2H_6,out} + n_{C_2H_4,out} + n_{CH_4,out}} \quad (3)$$

The catalytic activity of **$Pt^0Zn^{\delta+}/SiO_2$**, **Zn^{II}/SiO_2**, and **Pt^0/SiO_2** for propane dehydrogenation are summarized in figures S49-S52. The catalyst **$Pt^0Zn^{\delta+}/SiO_2$** was investigated at two WHSVs (h^{-1}) by varying the amount of catalyst (14.3 mg and 33.4 mg; Pt loading of 3 wt%) while maintaining identical gas composition and flow rate. In all cases conversions below equilibrium are achieved. Figure S51 shows product selectivity, propane conversion, and carbon balance at a WHSV of 75 h^{-1} for **$Pt^0Zn^{\delta+}/SiO_2$**. Figure S52 shows the same for a WHSV of 32 h^{-1}. Figure S50 shows product selectivity and propane conversion for **Pt^0/SiO_2** at WHSV 32 h^{-1} (33.4 mg, Pt loading of 3.96 wt%). Figure S49 shows product selectivity and propane conversion for **Zn^{II}/SiO_2** at WHSV 32 h^{-1} (33.4

mg; Zn loading of 1.6 wt%). Due to very low conversion levels the carbon balance was close to 100% in both cases. Propane dehydrogenation was also performed over SiC (2.5 g) at a flow of 50 mL/min with 20% C3H8/Ar yielding a conversion of 1.1% and the following selectivity: C_3H_6, 39.5%; C2H4, 29.8%; CH_4, 30.7%. $SiO_{2\text{-}700}$ (33.4 mg) dispersed in SiC (2.5 g) was also tested at a flow of 50 mL/min with 20% C3H8/Ar yielding a conversion of 1.2% and the following selectivity: C_3H_6, 38.4%; C_2H_4, 30.2%; C_2H_6, 0.1%; CH_4, 31.3%. The lower conversion of **Zn^{II}/SiO_2** compared to $SiO_{2\text{-}700}$ might be explained by the lower OH density on **Zn^{II}/SiO_2**.

Mass and Heat transfer limitation analysis[13]

$$Mears\ criterion\ (external\ mass\ transport): \quad \frac{-r(obs)\cdot\rho_b\cdot r\cdot n}{k_c\cdot c} < 0.15 \tag{4}$$

$$external\ heat\ transport: \quad \left|\frac{-\Delta H_r\cdot(-r(obs))\cdot\rho_b\cdot r\cdot E_a}{h_c\cdot T^2\cdot R}\right| < 0.15 \tag{5}$$

$$Weisz-Prater\ criterion\ (internal\ mass\ transport): \quad \frac{-r(obs)\cdot\rho_c\cdot r^2}{D_e\cdot c} \ll 1 \tag{6}$$

Table S8. List of catalyst process parameters

feature	value
Observed initial consumption rate per mass of catalyst: r(obs) (kmol/(kg_{cat} s))	$1.42\text{x}10^{-4}$
Bulk density of catalyst bed: $\rho_b=(1-\phi)\rho_c$ (kg/m^3)	1860
Porosity: ϕ[14]	0.38
Catalyst particle radius: r (m)	$2.25\text{x}10^{-4}$
Reaction order: n	1
Mass transfer coefficient: k_c (m/s)	0.268
reactant concentration: c (mol/dm^3)	$8.07\text{x}10^{-3}$
Heat of reaction: ΔH_r (kJ/mol)	124
Activation Energy: E_a (kJ/kmol)[doubled from 15]	200
Heat transfer coefficient between gas and pellet: h_c (kJ/(m^2 s K))	0.193
Reaction temperature: T (K)	823.15
Ideal gas constant: R (J/(mol K))	8.314
Solid density of catalyst pellet: ρ_c (kg/m^3)	3000
Effective diffusivity: (m^2/s)	$1.17\text{x}10^{-5}$
Mears number	**$2.75\text{x}10^{-2}$**
Heat transport number	**$1.36\text{x}10^{-6}$**
Weisz-Prater number	**$2.28\text{x}10^{-1}$**

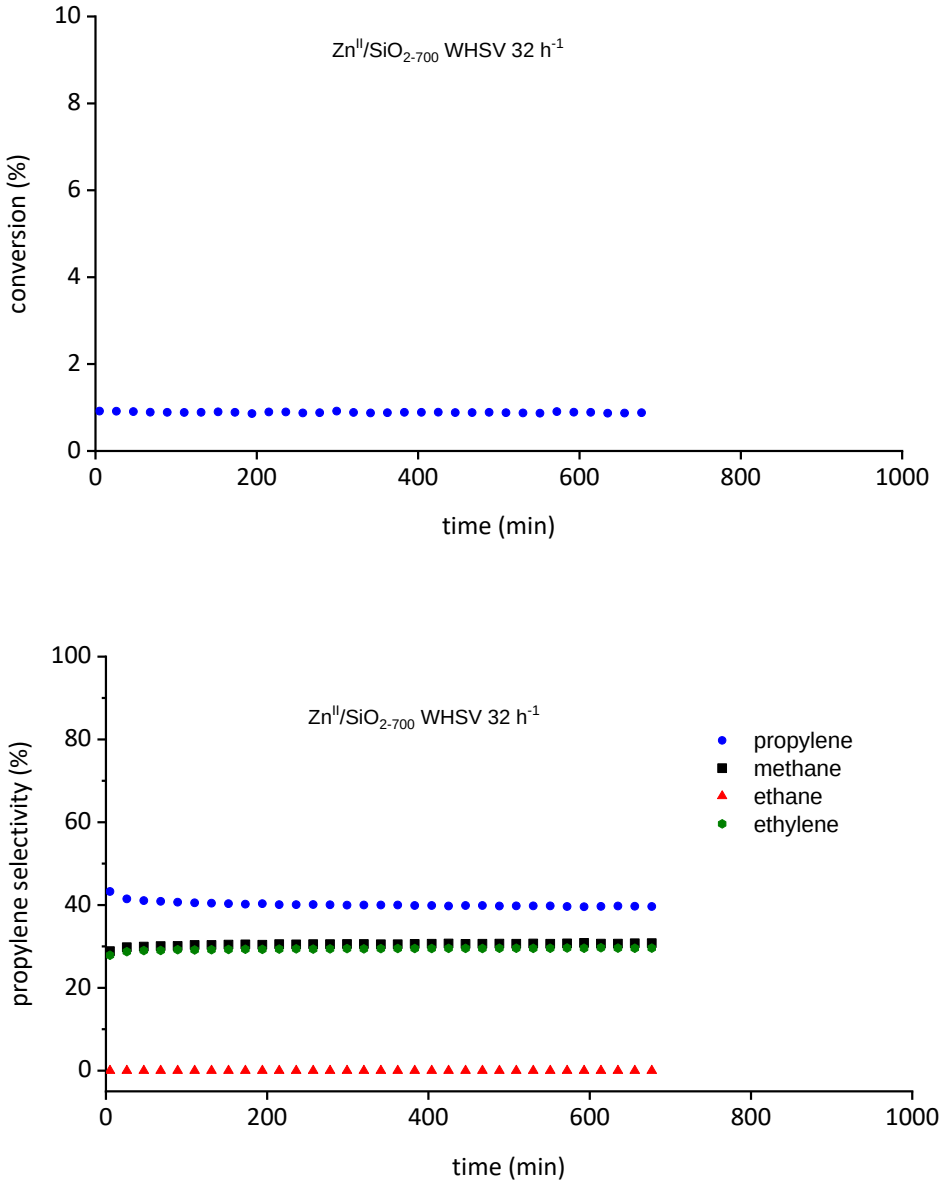

Figure S50. Upper: Propane Conversion of **Zn^{II}/SiO_2**. Lower: Product selectivity of **Zn^{II}/SiO_2**.

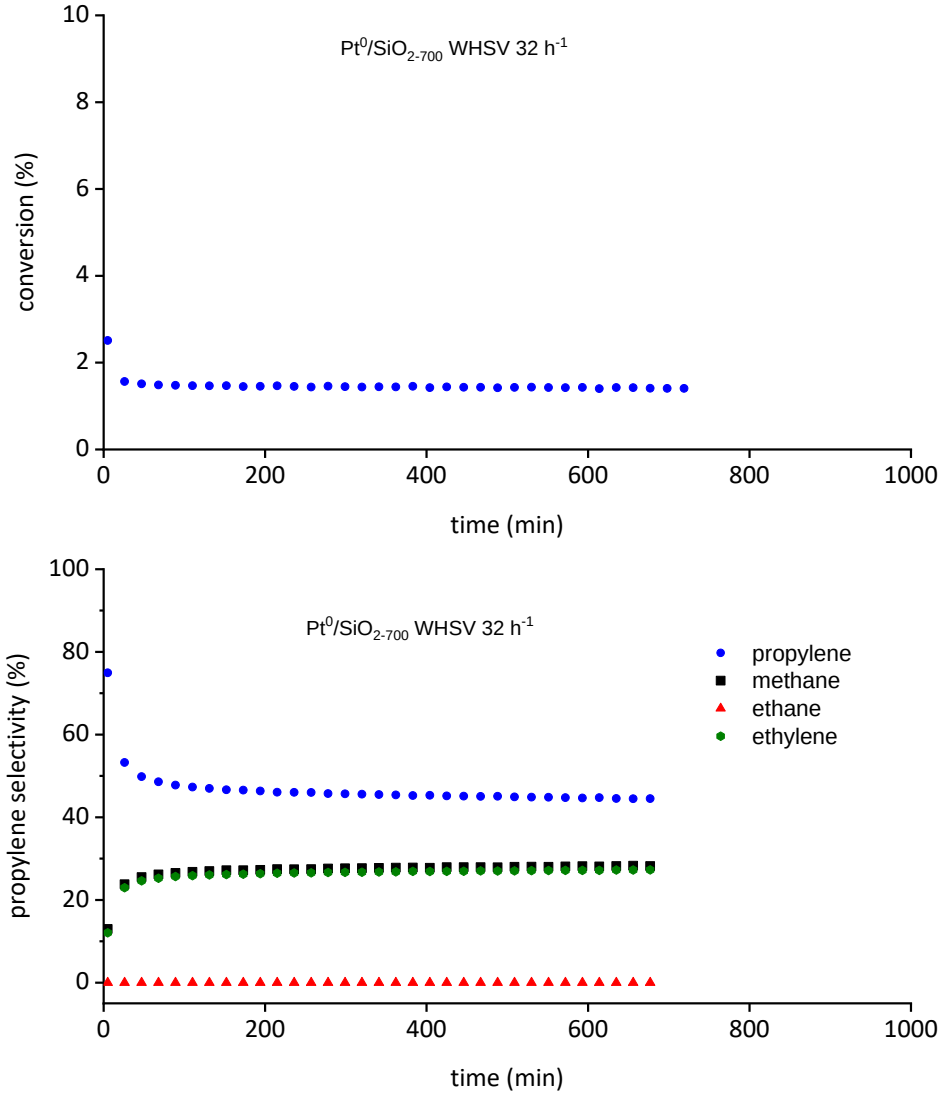

Figure S51. Upper: Propane Conversion of **Pt^0/SiO_2**. Lower: Product selectivity of **Pt^0/SiO_2**.

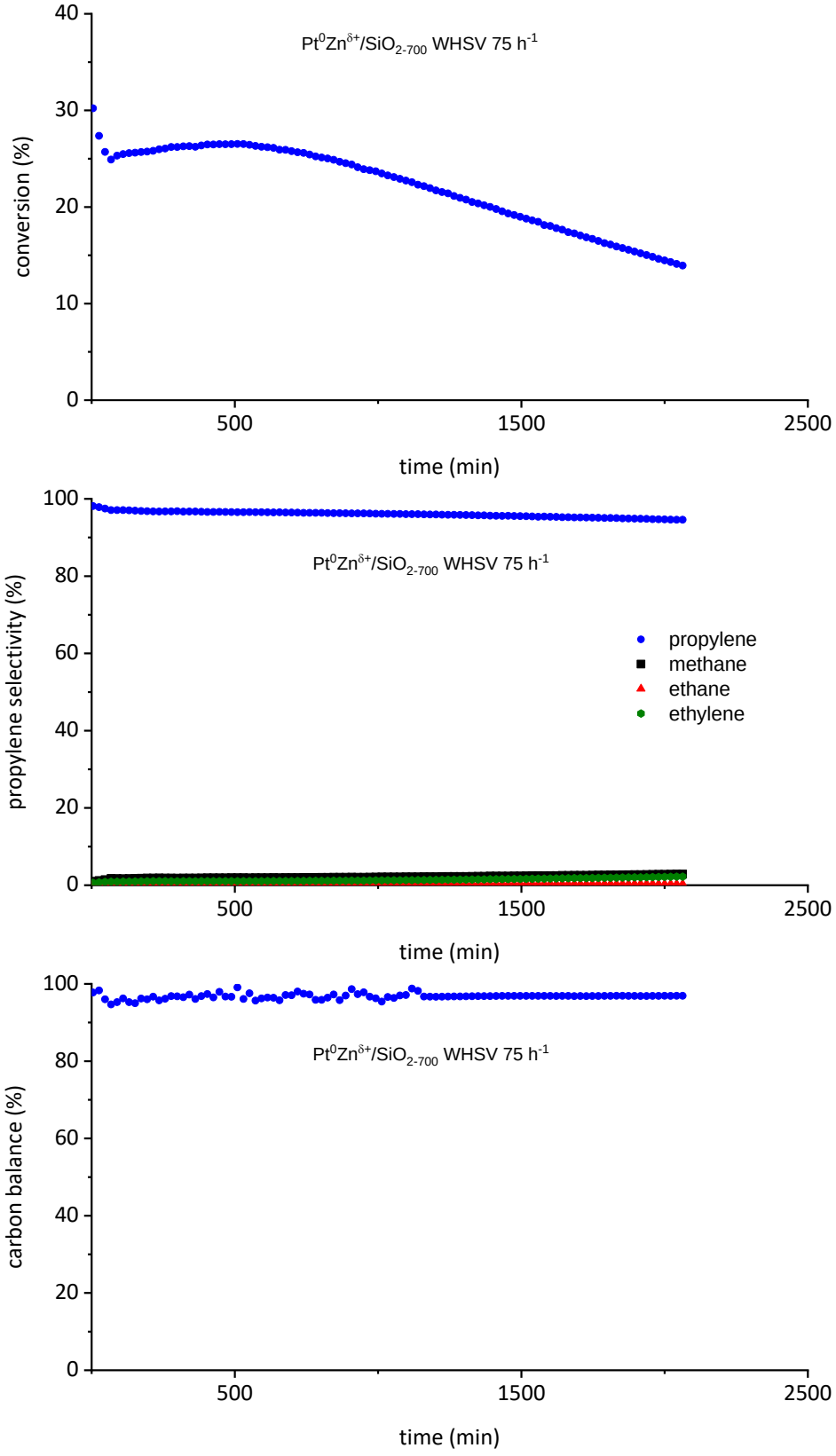

Figure S52. Upper: Propane Conversion of **$Pt^0Zn^{\delta+}/SiO_2$**. Middle: Product selectivity of **$Pt^0Zn^{\delta+}/SiO_2$**. Lower: Carbon balance of **$Pt^0Zn^{\delta+}/SiO_2$**.

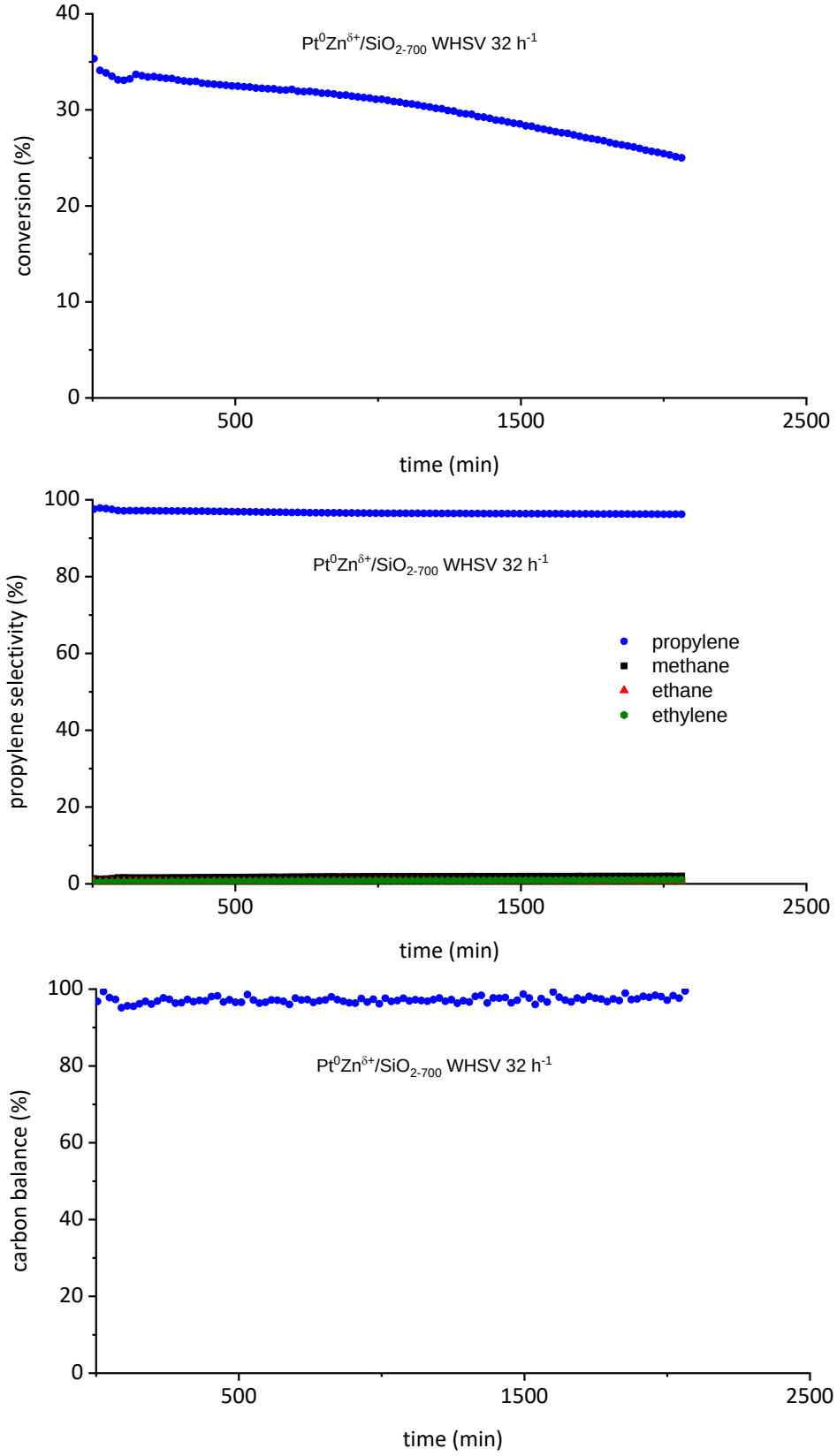

Figure S53. Upper: Propane Conversion of **$Pt^0Zn^{\delta+}/SiO_2$**. Middle: Product selectivity of **$Pt^0Zn^{\delta+}/SiO_2$**. Lower: Carbon balance of **$Pt^0Zn^{\delta+}/SiO_2$**.

Table S9. Comparison of catalytic performances for PDH between $Pt^0Zn^{\delta+}/SiO_2$ and other Pt-Zn based catalysts

sample	year	wt %	WHSV [h^{-1}]	T (°C)	C_3H_8:H_2 ratio	Reaction time (h)	Conversion (%)	Selectivity for C3H6 (%)	k_d (h^{-1})	Productivity (g_{C3H6} g_{Pt}^{-1} h^{-1})	Particle size [nm]
$Pt/ZnAl_2O_4$ (IMP)[16]	2000	Pt, 0.3 Zn, n/a	n/a	580	10:9	1.33	I: 22 F: 12.8	I: 94.5 F: 97	0.491	n/a	n/a
Pt/Zn-Beta (IE & IMP)[17]	2006	Pt, 0.5 Zn, 2.6	2.6	555	1:0	11	I: 40 F: 29	I: 30 F: 91	0.052	I: 60 F: 130	n/a
$PtZn/Al_2O_3$ (IMP)[18]	2007	Pt, 0.3 Zn, 0.5	n/a	576	1:1	2.6	I: 37.3 F: 24.2	I: 97.2 F: 98.9	0.239	n/a	n/a
$PtZn/MgAl_2O_4$ (IMP)[19]	2009	Pt, 0.3 Zn, n/a	1.75	530	1:1	5	I: 27.5 F: 10.0	I: 93.8 F: 99	0.246	I: 143 F: 56.7	3.9
$PtSnZn/Al_2O_3$ (FSP)[20]	2011	Pt, 0.3 Zn, 0.5	5	550	1:1	3	I: 8.6 F: 8.1	I: 76	0.023	I: 103	n/a
$PtSn/ZnAl_2O_4$ (IWI)[21]	2011	Pt, 3.0 Zn, n/a	32	600	1:0	4	I: 44 F: 20	I: 90 F: 97	0.286	I: 403 F: 197.7	n/a
PtNaZn/ZSM-5 (IMP)[22]	2015	Pt, 0.5 Zn, 1.0	3.0	590	4:1	10	I: 40.6 F: 37.7	I: 93 F: 97	0.012	I: 216 F: 210	n/a
$PtZn/Al_2O_3$ (IWI)[23]	2016	Pt, 0.1 Zn, 15	3.0	600	1:1	4	I: 35 F: 31	I: 94 F: 97	0.045	I: 770 F: 640	n/a
Pt/MgZnAlOx (IMP)[24]	2016	Pt, 0.3 Zn, >30	6.4	550	4:1	4	I: n/a F: 20.0	I: n/a F: 99	n/a	n/a	~1.7
$Pt^0Zn^{\delta+}/SiO_2$	2019	Pt, 3.0 Zn, 1.5	75	550	1:0	30	I: 30.2 F: 16.1	I: 98.1 F: 95.0	0.027	I: 703 F: 375	0.8±0.2

TGA studies.

TGA measurements were performed using a PerkinElmer TGA7 instrument. Approximately 5-10 mg of each sample contained in an Al_2O_3 crucible was heated from 35 to 800 °C at a rate of 20 °C/min under a flow of synthetic air (20 % O2/Ar). Onset temperatures for the samples were around 500 °C. We exemplarily show the data for the sample at WHSV of 75 h^{-1}. A single mass spec signal at 44 amu (CO_2) could be detected during mass loss, indicative for the removal of coke from the materials surface.

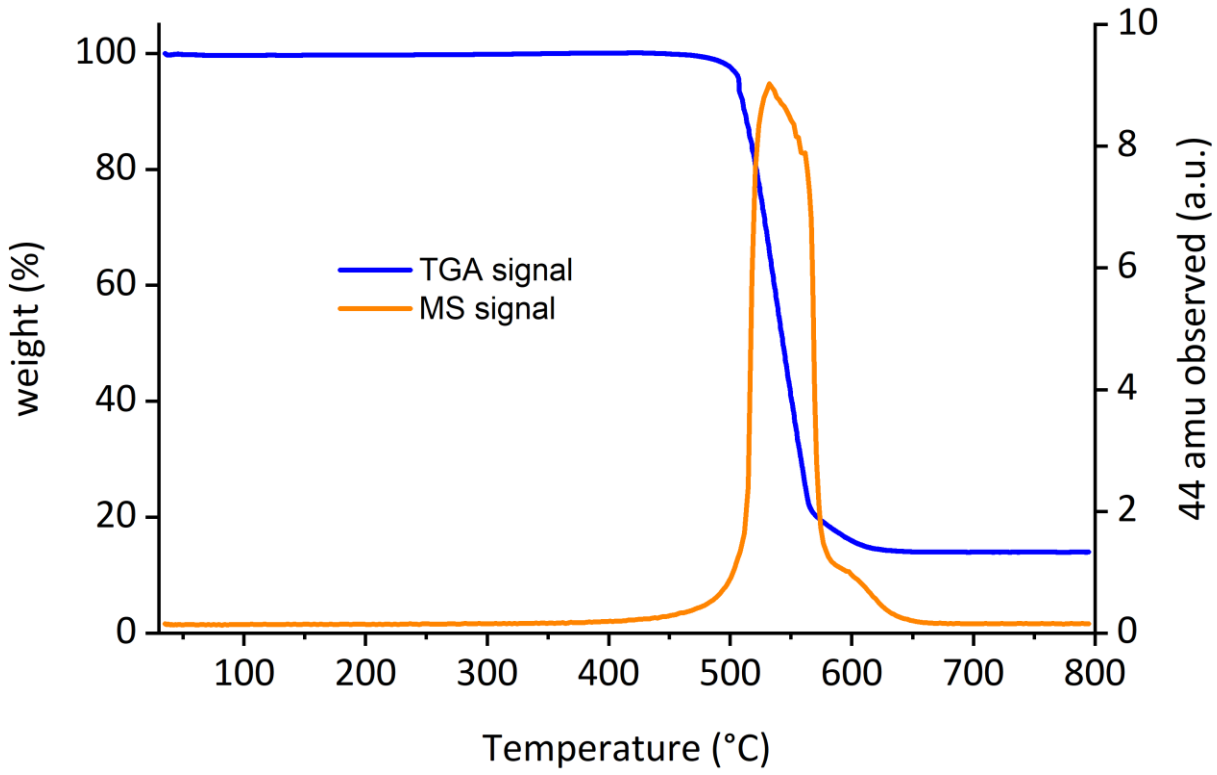

Figure S54. Weight loss analysis (TGA) and corresponding observed MS signal (44 amu) of **$Pt^0Zn^{\delta+}/SiO_2$** after 30 h on stream.

References

1 K. Su, T. D. Tilley and M. J. Sailor, *J. Am. Chem. Soc.*, 1996, **118**, 3459–3468.

2 D. A. Ruddy, J. Jarupatrakorn, R. M. Rioux, J. T. Miller, M. J. McMurdo, J. L. McBee, K. A. Tupper and T. D. Tilley, *Chem. Mater.*, 2008, **20**, 6517–6527.

3 A. K. Cook and C. Copéret, *Organometallics*, 2018, **37**, 1342–1345.

4 P. Laurent, L. Veyre, C. Thieuleux, S. Donet and C. Copéret, *Dalt. Trans.*, 2013, **42**, 238–248.

5 C. Morterra and G. Cerrato, *Catal. Letters*, 1991, **10**, 357–363.

6 B. A. Morrow, I. A. Cody, L. E. Moran and R. Palepu, *J. Catal.*, 1976, **44**, 467–476.

7 S. Haq and D. A. King, *J. Phys. Chem.*, 1996, **100**, 16957–16965.

8 R. Ferwerda, J. H. van der Maas and F. B. van Duijneveldt, *J. Mol. Catal. A Chem.*, 1996, **104**, 319–328.

9 K. Searles, K. W. Chan, J. A. Mendes Burak, D. Zemlyanov, O. Safonova and C. Copéret, *J. Am. Chem. Soc.*, 2018, **140**, 11674–11679.

10 O. Müller, J. Stötzel, D. Lützenkirchen-Hecht and R. Frahm, *J. Phys. Conf. Ser.*, 2013, **425**, 092010.

11 B. Ravel and M. Newville, *J. Synchrotron Radiat.*, 2005, **12**, 537–541.

12 H. Nowotny, E. Bauer and A. Stempfl, *Monatshefte für Chemie*, 1950, **81**, 1164–1164.

13 H. S. Fogler, *Elements of chemical reaction engineering*, Prentice Hall, 4th edn., 2006.

14 A. S. Pushnov, *Chem. Pet. Eng.*, 2006, **42**, 14–17.

15 J. T. Miller, V. J. Cybulskis, B. C. Bukowski, H.-T. Tseng, J. R. Gallagher, Z. Wu, E. Wegener, A. J. Kropf, B. Ravel, F. H. Ribeiro and J. Greeley, *ACS Catal.*, 2017, **7**, 4173–4181.

16 S. R. de Miguel, E. L. Jablonski, A. A. Castro and O. A. Scelza, *J. Chem. Technol. Biotechnol.*, 2000, **75**, 596–600.

17 P. L. De Cola, R. Gläser and J. Weitkamp, *Appl. Catal. A Gen.*, 2006, **306**, 85–97.

18 C. Yu, H. Xu, Q. Ge and W. Li, *J. Mol. Catal. A Chem.*, 2007, **266**, 80–87.

19 Y. Wang, Y. Wang, S. Wang, X. Guo, S.-M. Zhang, W.-P. Huang and S. Wu, *Catal. Letters*, 2009, **132**, 472–479.

20 S. Pisduangdaw, J. Panpranot, C. Chaisuk, K. Faungnawakij and O. Mekasuwandumrong, *Catal. Commun.*, 2011, **12**, 1161–1165.

21 B. K. Vu, M. B. Song, I. Y. Ahn, Y.-W. Suh, D. J. Suh, W.-I. Kim, H.-L. Koh, Y. G. Choi and E. W. Shin, *Appl. Catal. A Gen.*, 2011, **400**, 25–33.

22 Y. Zhang, Y. Zhou, L. Huang, S. Zhou, X. Sheng, Q. Wang and C. Zhang, *Chem. Eng. J.*, 2015, **270**, 352–361.

23 G. Liu, L. Zeng, Z.-J. Zhao, H. Tian, T. Wu and J. Gong, *ACS Catal.*, 2016, **6**, 2158–2162.

24 O. B. Belskaya, L. N. Stepanova, T. I. Gulyaeva, S. B. Erenburg, S. V. Trubina, K. Kvashnina, A. I. Nizovskii, A. V. Kalinkin, V. I. Zaikovskii, V. I. Bukhtiyarov and V. A. Likholobov, *J. Catal.*, 2016, **341**, 13–23.